

1 Influence of vertical heterogeneities in the canopy microenvironment on inter-
2 annual variability of carbon uptake in temperate deciduous forests

3 **M. C. Wozniak^{1,*}, G. B. Bonan², G. Keppel-Aleks¹, and A. L. Steiner¹**

4 ¹ Department of Climate and Space Sciences and Engineering, University of Michigan, Ann
5 Arbor, MI, USA.

6 ² National Center for Atmospheric Research, P.O. Box 3000, Boulder, Colorado, 80307, USA

7 * Now at: Program in Atmospheric and Oceanic Sciences, Princeton University, Princeton, NJ,
8 USA

9 Corresponding author: Matthew C. Wozniak (mwozniak@princeton.edu)

10 **Key Points:**

- 11 • Explicitly simulated leaf area and microclimatic profiles do not affect gross primary
12 productivity (GPP) inter-annual variability compared to a “big-leaf” simplification.
- 13 • Multilayer plant hydraulics lead to vertically varying water stress, altering leaf-layer
14 responses to inter-annual climate variations.
- 15 • All model simulations underestimate hourly GPP compared to FLUXNET estimates,
16 adversely impacting simulated GPP inter-annual variability.

This is the author manuscript accepted for publication and has undergone full peer review but has not been through the copyediting, typesetting, pagination and proofreading process, which may lead to differences between this version and the [Version of Record](#). Please cite this article as doi: [10.1029/2020JG005658](https://doi.org/10.1029/2020JG005658)

17 **Abstract**

18 Vegetation structure and function are key design choices in terrestrial models that affect the
19 relationship between carbon uptake and environmental drivers. Here, we investigate how
20 representing canopy vertical structure in a terrestrial biosphere model - i.e. micrometeorological,
21 leaf area and leaf water profiles - influences carbon uptake at five U.S. temperate deciduous
22 forest sites in July. Specifically, we test whether the inter-annual variability (IAV) of gross
23 primary productivity (GPP) responds differently to four abiotic environmental drivers – air
24 temperature, relative humidity, incoming shortwave radiation and soil moisture – using either a
25 multi-layer canopy model (CLM-ml) or a big-leaf model (CLM4.5/CLM5). We conclude that
26 vertical leaf area and microclimatic profiles (temperature, humidity and wind) do not impact
27 GPP IAV compared to a single-layer model when plant hydraulics are excluded. However, with
28 a mechanistic representation of plant hydraulics there is vertically varying water stress in CLM-
29 ml, and the sensitivity of carbon uptake to particular climate variables changes with height,
30 resulting in dampened canopy-scale GPP IAV relative to CLM4.5. Dampening is due to both a
31 reduced dependence on soil moisture and opposing climatic forcing on different leaf layers. Such
32 dampening is not evident in the single-layer representation of plant hydraulic water stress
33 implemented in the recently released CLM5. Overall, both model representations of the canopy
34 fail to accurately simulate observed GPP IAV and this may be related by their inability to capture
35 the upper range of observed hourly GPP and diffuse light-GPP relationships that cannot be
36 resolved by canopy structure alone.

37

38 **1 Introduction**

39 Inter-annual variability (IAV) in the growth rate of atmospheric CO₂ concentrations is
40 largely dependent on the variability of the land sink (Keeling et al. 1995; Schimel et al. 2001;
41 Nevison et al. 2008; Le Quere et al. 2017), and the land sink is closely coupled to climate
42 variability (Beer et al. 2010; Poulter et al. 2014; Ahlstrom et al. 2015; Sitch et al. 2015; Fu et al.
43 2017; Rodenbeck et al. 2018). A quantitative understanding of the relationship between climate
44 variations and the land sink response is therefore crucial for accurate prediction of carbon-
45 climate feedbacks. Because photosynthesis represents the pathway by which carbon enters
46 terrestrial ecosystems, understanding the sensitivity of this process to environmental drivers is
47 necessary to constrain the terrestrial carbon sink (Anav et al. 2015). The environmental drivers of

48 photosynthesis – temperature, moisture, and radiation – often covary. For example, drought
49 conditions usually reflect both low precipitation and high temperature, while above-average
50 precipitation likely co-occurs with high cloud cover, which reduces radiation. These covariances
51 make it difficult to unambiguously attribute variations in gross primary productivity (GPP) to the
52 underlying driver.

53 Terrestrial biosphere models are one way the disambiguation of carbon cycle processes
54 can be achieved. Earth system models (ESMs) equipped with terrestrial biosphere models can
55 simulate the evolution of the terrestrial carbon sink under climate change and the sink’s coupling
56 with climate (Anav et al. 2013; Arora et al. 2013). However, modeling estimates of the inter-
57 annual variability of the terrestrial carbon sink diverge due to the uncertainty in terrestrial model
58 processes (Keenan et al. 2012; Bonan and Doney 2018). Some of this uncertainty results from
59 simplifications in representing ecological processes within land models. For example, most
60 ESM land components simulate the vegetation canopy as a simplified single bulk leaf layer, or
61 “big-leaf,” that exchanges mass and energy with the atmosphere (Sinclair, Murphy & Knoerr
62 1976). In reality, vertical structure in the tall canopies of forests may influence the response of
63 carbon uptake to variability in these drivers, including on the inter-annual scale.

64 Forest canopies, including temperate deciduous canopies, exhibit considerable structural
65 heterogeneity from the top to the bottom that impacts the within-canopy physical environment,
66 particularly light extinction, microclimate, and leaf water stress. Leaf area density, leaf angle and
67 other canopy architectural traits (for example, clumping) also vary with height in forest canopies
68 (Parker, O’Neill & Higman 1989; Niinemets 1998; Walcroft et al. 2005; Zhao et al. 2011). Such
69 vertical architectural heterogeneity can affect radiation extinction from successive canopy
70 shading, and potentially lead to diurnal, seasonal or spatial differences in carbon uptake
71 depending on canopy structure (Koike et al. 2001; Funk and Ler dau 2004; Parker et al. 2005;
72 Niinemets & Valladares 2004). The interactions between canopy architecture, the varied light
73 environment and within-canopy turbulence produce a vertically varied microclimate (Elias et al.
74 1989; Flerchinger et al. 2015) capable of moderating weather and climatic extremes (Carlson &
75 Groot 1997; Chen et al. 1999; Rambo & North 2009; Von Arx, Dobbertin & Rebetez 2012; Du
76 Frenne et al. 2013). Because photosynthesis is tightly coupled with meteorological conditions,
77 carbon uptake in canopies is sensitive to vertical light and meteorological gradients and the
78 interactions between such gradients, particularly during meteorological extremes (Niinemets &

79 Valladares 2004).

80 Vertically resolved multilayer canopy models have been applied to vegetation-
81 atmosphere carbon fluxes in forests and other plant canopies to resolve the impacts of vertical
82 heterogeneity in canopy architecture and environmental conditions (Baldocchi, Wilson and Gu
83 2002; Wu et al. 2003; Walcroft et al. 2005; Drewry et al. 2010; Bonan et al. 2014; Bonan et al.
84 2018; Chang et al. 2018). For example, a recent study using the Advanced Canopy-Atmosphere-
85 Soil Algorithm (ACASA) model concluded that resolved scalar profiles (temperature, humidity
86 and carbon dioxide) reduced canopy carbon uptake by an average of 10%, and that the multilayer
87 model improved simulated daily fluxes compared to a single layer model at sites where seasonal
88 variability in canopy structure (leaf area index) was great (Chang et al. 2018). Drewry et al.
89 (2010) and Wu et al. (2003) both analyzed the sensitivity of canopy CO₂ fluxes to meteorological
90 conditions, and found that modeled CO₂ flux was sensitive to vertical temperature gradient.
91 Walcroft et al. (2005) found that vertically-varied clumping (i.e. overlap of leaves) increased
92 simulated canopy photosynthesis by 12% relative to randomly distributed leaves. Finally, Bonan
93 et al. (2014) found that including vertically-resolved plant hydraulics and water stress improved
94 the simulated diurnal cycle of GPP in forests that were water stressed, and postulated that
95 vertical canopy profiles may be important for accurately simulating vegetation-atmosphere
96 fluxes. These studies show that vertical representation in canopy models could be important to
97 photosynthetic carbon uptake and its response to the environment.

98 Adding further complexity to a forest canopy is the hydraulic architecture of plants by
99 which soil water is transferred to leaves to maintain moisture during photosynthesis (Tyree and
100 Ewers 1991). Plant hydraulic stress occurs when xylem water potential drops below a threshold
101 that causes a loss in hydraulic conductivity within the plant. Observational studies show that
102 plant hydraulic adaptation to water stress may be important for photosynthetic performance in
103 relationship to water availability (Taylor & Eamus 2008; Zhang & Cao 2009; Aranda et al.
104 2014). Therefore, vegetation models may benefit from more realistic plant hydraulic trait-based
105 carbon-water coupling, such as accounting for stomatal responses to reduced xylem pressure
106 (e.g. Bonan et al. 2014). Plant hydraulic stress is not distributed evenly throughout the canopy,
107 though, as water potential varies with the vertical canopy light gradient because of covarying leaf
108 temperature and vapor pressure deficit (Hellkvist, Richards and Jarvis 1974; Niinemets &
109 Valladares 2004). Models that parameterize this behavior have shown that including plant

110 hydraulics creates vertical variation in stomatal conductance according to a balance between
111 radiative intensity and leaf water status (e.g. Williams et al. 1996). In the multi-layer canopy
112 study by Drewry et al. (2010), the sensitivity of photosynthesis to water stress was dampened in
113 soybean and maize canopies when leaf stomatal conductance was linked to root zone water stress
114 via plant hydraulics, instead of linking stomatal conductance directly to soil moisture. Their
115 results also show the non-uniform soybean canopy was more greatly impacted by water stress in
116 the upper canopy where leaf area density peaked. While models (e.g. CLM5, CLM-ml; Bonan et
117 al. 2014; Kennedy et al. 2019) have begun to depart from arbitrary soil moisture stress
118 parameterizations in favor of parameterizations that modulate photosynthesis and
119 evapotranspiration via plant hydraulic traits, the impacts of such an advancement on canopy
120 carbon uptake should be carefully examined against observations at multiple timescales, as well
121 as the differential impacts of plant hydraulic stress in big-leaf versus multi-layer canopy models.

122 To date, the difference between multilayer and big-leaf representations of a forest canopy
123 regarding their simulation of the response of photosynthesis to inter-annual climate variations,
124 particularly when canopy architecture, microclimate, and hydraulic status vary along a vertical
125 gradient, has not been demonstrated. Here, we evaluate modeled IAV in peak summer GPP in
126 big-leaf and multilayer models, and investigate the extent to which vertical heterogeneity
127 resolved in a multilayer model affects the simulated GPP response to climate IAV. We further
128 investigate whether representing vertically varying water stress within the multi-layer canopy
129 affects the direct response of photosynthesis to inter-annual soil moisture stress. For this
130 analysis, we compare two versions of a multilayer model (one keeping soil moisture stress
131 constant at each canopy layer, one that varies soil moisture stress) with similar big-leaf models at
132 five temperate deciduous broadleaved forest (DBF) FLUXNET sites in the Northeastern US. We
133 focus on these forests because temperate forests are a growing carbon sink and their sensitivity to
134 climate fluctuations may affect the future of the Northern Hemisphere land sink (Pan et al. 2011;
135 Shiga et al. 2018). Photosynthesis is a multivariate response; thus, we use four environmental
136 variables (temperature, humidity, radiation and soil moisture) to represent climate IAV. The
137 model results are interpreted with an observationally based GPP product from eddy-covariance
138 flux tower measurements, and the sensitivity of these results to diffuse light representation in the
139 multilayer model is also examined by using diffuse light measurements from one of the flux
140 towers. The implications for carbon-climate coupling in terrestrial forest ecosystems are

141 discussed.

142

143 **2 Data and methods**

144 ***2.1 FLUXNET eddy covariance data***

145 FLUXNET is a global network of eddy covariance towers that measure the flux of
146 energy, water and CO₂ between the ecosystem and atmosphere (Williams et al. 2009; Pastorello
147 et al. 2017). We analyze data from five temperate deciduous broadleaved forest (DBF)
148 FLUXNET sites in the eastern United States with about a decade or more of data. Harvard Forest
149 (US-Ha1; 42.54 N, 72.17 W; 1991-2012; DOI: 10.18140/FLX/1440071) is majority red oak and
150 red maple, mixed with hemlock and white pine. The tower and canopy heights are 30 m and 23
151 m, respectively. Morgan-Monroe State Forest (US-MMS; 39.32 N, 86.41 W; 1999-2014; DOI:
152 10.18140/FLX/1440083) is a secondary successional forest located across a maple-beech to oak-
153 hickory transition zone. Its tower and canopy heights are 48 m and 27 m, respectively. The Oak
154 Openings tower is located within an oak woodland dominated by red, white and black oak, as
155 well as red maple (US-Oho; 41.55 N, 83.84 W; 2004-2013; DOI: 10.18140/FLX/1440088), with
156 tower and canopy heights of 32 m and 24 m. University of Michigan Biological Station (US-
157 UMB; 45.56 N, 84.71 W; 2000-2014; 10.18140/FLX/1440093) is predominantly aspen, but the
158 footprint also contains red oak, red maple, and beech, as well as some hemlock and white pine.
159 Its tower and canopy heights are 46 m and 21 m, respectively. Finally, Willow Creek is
160 dominated by sugar maple and basswood (US-WCr; 45.81 N, 90.08 W; 1999-2014; DOI:
161 10.18140/FLX/1440095) with tower and canopy heights of 48 m and 24 m.

162 Direct meteorological measurements with gap filling are available from each tower and
163 include air temperature and pressure, wind speed, vapor pressure deficit (VPD), net shortwave
164 (SW) and longwave radiative fluxes, and precipitation flux. These measurements are used both
165 as atmospheric forcing for the CLM simulations described below (e.g., Pastorello et al. 2017)
166 and for the regression analysis described in Section 2.3. Gap-filled daytime-partitioned GPP
167 estimates used here are from the FLUXNET2015 dataset, and are hereafter referred to as
168 “observed” GPP (Lasslop et al. 2012). Nighttime-partitioned GPP estimates are also available
169 from the FLUXNET2015 dataset, and for some site-years (e.g. 1997 at US-Ha1; 2003-2004 at
170 US-MMS) the nighttime estimate differs substantially (Figure S1). However, most of the data
171 from the nighttime-partitioned GPP are within error of the daytime-partitioned estimates based

172 on random error in carbon flux measurements reported for FLUXNET eddy covariance towers,
173 which is about 20% (Richardson et al. 2006; shading in Figure S1). Each site has a history of
174 disturbances that have occurred throughout the measurement period, some of which may have
175 affected GPP at the inter-annual timescale. At US-Ha1, there was an ice storm in the winter of
176 2008-2009 that caused some canopy damage, including a loss of 1.5 MgC ha⁻² of woody debris
177 and a reduction of LAI by 1.4 m² m⁻². At US-MMS, there was a flood in June 2012 succeeded by
178 drought in July of 2012 directly affecting July GPP, while some insect damage occurred in 2004
179 and following the 2012 drought (with minimal impact). At US-WCr, there was a tent caterpillar
180 outbreak in June 2001 causing full defoliation, with leaf recovery in July 2001, and a 30% forest
181 overstory thinning in 2013-2014. The potential impact of these disturbances on the results is
182 discussed in Section 3.2.

183 Because the model simulations (described in Section 2.2) require atmospheric relative
184 humidity (RH) input and only VPD data are available without gaps, VPD is converted to relative
185 humidity using an empirical estimate of saturation vapor pressure via Murray (1967). This
186 calculation sometimes results in negative RH values, which are replaced by linearly interpolating
187 between the nearest positive neighbors. Root-zone soil water content (SWC) measurements are
188 available at all FLUXNET sites except US-Ha1. In addition to the FLUXNET2015 data
189 described above, we also use diffuse and total photosynthetic active radiation (PAR)
190 measurements at US-UMB to explore the role of diffuse light on carbon uptake (see Section 2.4
191 for methodology). Diffuse and total PAR are measured by a BF2 (2004-2012) or BF5 (2013-
192 2014) Sunshine Sensor at the US-UMB FLUXNET tower for a total period of 2004-2014, which
193 coincides with the FLUXNET2015 dataset.

194 195 **2.2 Land model simulations**

196 We used a suite of Community Land Model (CLM) versions (Table 1) to simulate July
197 GPP IAV at the sites described above. In this analysis, we focus on how the differences in
198 vertical canopy structure and water stress parameterization between big-leaf and multilayer CLM
199 variants affect GPP. When similar parameterizations are used, the model variants use the same
200 parameters for biogeophysical processes, and it is through these similarities that we seek to
201 minimize intermodel parametric and structural differences arising from other factors. For
202 example, the multilayer version of CLM (CLM-ml) was developed as an experimental branch of

203 the CLM to test hypotheses related to a multilayer canopy representation. While some of its
 204 physics are by necessity formulated differently from the standard CLM, much of the model
 205 structure is adopted from the previous community release of CLM (version 4.5, see Section
 206 2.2.1) and a comparison of these two model versions isolates the impact of only a few new
 207 physical parameterizations. The newest community release of CLM (CLM5) exhibits several
 208 differences compared with CLM4.5, thus we mainly compare two configurations of CLM5
 209 against one another (see Section 2.2.3). We note that this study does not address parametric
 210 uncertainty at the individual sites or for individual species for any of the models; however, the
 211 impact of parametric uncertainty on the results is discussed in Section 4. The models and
 212 simulations are described in detail below.

Simulation	Canopy type	Soil moisture	Stomatal conductance	Water stress type	Reference for model
CLM4.5	Big-leaf	Simulated and coupled with canopy	Ball-Berry (Collatz et al. 1991)	Soil moisture stress factor, β_t	Oleson et al. 2013
CLM-ml-BB	Multilayer	Prescribed from CLM4.5 run	Ball-Berry (Collatz et al. 1991)	Soil moisture stress factor, β_t	Bonan et al. 2014; Bonan et al. 2018
CLM-ml-SPA	Multilayer	Prescribed from CLM4.5 run	Water use efficiency (Williams et al. 1996; Bonan et al. 2014)	Plant hydraulic stress via minimum leaf water potential threshold, $\psi_{l,\min}$ (Williams et al. 1996; Bonan et al. 2014)	Bonan et al. 2014; Bonan et al. 2018
CLM5-PHS	Big-leaf	Simulated and coupled with canopy	Medlyn (Medlyn et al. 2011)	Plant hydraulic stress via water potential threshold for 50% xylem conductivity, P_{50} , embedded in water stress factor, f_w	Lawrence et al. 2019

				(Kennedy et al. 2019)	
CLM5-noPHS	Big-leaf	Simulated and coupled with canopy	Ball-Berry (Collatz et al. 1991)	Soil moisture stress factor, β_t	Lawrence et al. 2019

Table 1. Model configuration descriptions for each simulation.

2.2.1 Big-leaf model: CLM4.5

Community Land Model version 4.5 (CLM4.5) is the land surface model within the Community Earth System Model version 1.2 (CESM1.2) (Oleson et al. 2013). CLM simulates biogeophysical and biogeochemical processes that control exchanges of energy, water, and momentum between the soil, plant canopy and atmosphere. Vegetation is represented by plant functional types (PFTs), and the canopy in CLM4.5 is modeled as a single, bulk leaf layer, i.e. a “big-leaf” canopy. The big leaf is apportioned into a sunlit fraction that absorbs direct and diffuse light and a shaded fraction that absorbs diffuse light only. The sunlit and shaded fractions are characterized by their own photosynthesis and stomatal conductance, but canopy temperature and energy fluxes are calculated using an aggregate canopy conductance. Surface layer dynamics controlling momentum, sensible heat and latent heat fluxes are given by Monin-Obukhov Similarity Theory (MOST) (Zeng & Dickinson 1998). Photosynthesis (for C_3 plants) is modeled using the Farquhar (1980) model, and stomatal conductance is simulated by the Ball-Berry model described in Collatz et al. (1991). Water stress is simulated with a soil moisture stress parameter, β_t , which varies from 0 to 1 according to soil water matric potential and scales the minimum stomatal conductance parameter and also photosynthetic rates. Surface hydrology is represented by a variety of parameterizations simulating several fluxes (e.g. canopy interception and throughfall, evaporation, infiltration, etc.) that contribute to the surface water balance, given by the following equation,

$$(1) \quad \Delta W_{canopy} + \Delta W_{surface} + \Delta W_{snow} + \Delta W_{aquifer} + \sum_{soil\ levels} (\Delta w_{liq} + \Delta w_{ice}) = \Delta t [q_{rain} + q_{snow} - q_{overflow} - q_{drainage} - q_{runoff} - E_{vegetation} - E_{ground}],$$

where each ΔW is the change in water storage in the canopy, at the surface, in the snowpack, in an unconfined aquifer underneath the soil layers, respectively; while each Δw is the change in soil liquid and solid water content at each soil layer, summed over soil layers. The change in total water storage during each timestep, Δt , depends on the strength of liquid water and

241 evaporative fluxes represented by q and E , respectively. A detailed description of the individual
242 parameterizations for each hydrological process is provided in Oleson et al. (2013).

243 CLM4.5 simulations are run in offline, “single point” mode to simulate the fluxes at an
244 eddy covariance flux tower, and use meteorological observations from the tower as atmospheric
245 boundary conditions. Simulations are run for the years of data available at each site. A
246 representative PFT is used for each site (in this case DBF at all sites), and only the canopy and
247 soil biogeophysical processes are simulated in response to the atmospheric forcing. Phenology,
248 or the seasonal evolution in leaf area index (LAI), is derived from satellite data and is prescribed
249 as a climatological monthly mean without IAV (Lawrence and Chase 2007). The default
250 biogeophysical parameters for DBF are used (Oleson et al. 2013), and ambient CO₂ is held
251 constant at 360 ppm. All CLM4.5 simulations are initialized from the same “arbitrary initial
252 conditions,” which are preselected in the CLM code (Oleson et al. 2013, pp. 27). For the land
253 surface, this means that moisture is initialized at 0.15 m³ m⁻³ and soil temperature at 274 K
254 throughout the soil column, while vegetation temperature is initialized at 283 K. These
255 simulations provide a standard big-leaf baseline for simulation of the response of GPP to climate,
256 and also simulated soil moisture for prescription in CLM-ml (see Section 2.2.2).

257

258 2.2.2. Multilayer model: CLM-ml

259 We use a multilayer version of CLM (CLM-ml) to test the impacts of resolving the
260 vertically-structured canopy microenvironment on the IAV of carbon uptake in forests (Bonan et
261 al. 2014, 2018). CLM-ml models the canopy as a stack of thin (0.5 m) big-leaf layers, each
262 divided into sunlit and shaded fractions with unique leaf-level characteristics (e.g. leaf
263 temperature, stomatal conductance). Leaf area index varies with height according to a beta
264 distribution function (dLAI in Figure 1e) for a typical DBF canopy, which we refer to as a non-
265 uniform distribution throughout the paper. Each bulk leaf layer is associated with and exchanges
266 fluxes with an individual atmospheric layer, which in turn communicates with each neighboring
267 atmospheric layer. Scalar profiles (wind speed, temperature and vapor pressure) are computed
268 using a set of coupled flux-profile equations that account for canopy-induced turbulence above
269 and within the canopy (Bonan et al. 2018).

270

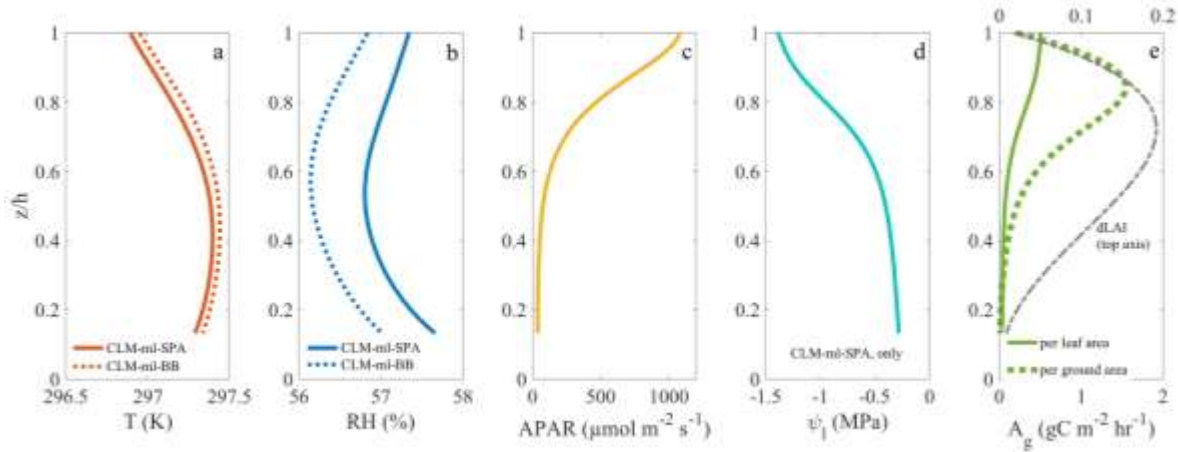


Figure 1. Mean daytime vertical profiles in CLM-ml (US-UMB) (averaged over 10am-4pm over 2001-2014) for **a)** air temperature (T), **b)** relative humidity (RH), **c)** absorbed photosynthetic active radiation (APAR), **d)** leaf water potential (LWP, here ψ_l), and **e)** gross carbon assimilation rate (A_g) and leaf area density (dLAI) distribution (top axis). z/h is relative height within canopy of height h .

CLM-ml has two representations for photosynthesis-stomatal conductance coupling and water stress: (1) a conventional, empirical model (Ball-Berry, β_i ; same as CLM4.5 but with β_i applied equally at all leaf layers) and the (2) the soil-plant-atmosphere model (SPA; Williams et al., 1996; Williams et al. 2001). When the water potential in vegetation leaves, and by consequence in the stem, drops due to water stress, cavitation (i.e. dissolution of air and bubble formation) occurs and can lead to embolism (i.e. complete blockage to flow). Trees prevent this by closing their stomates before the negative pressure grows intense enough to cause cavitation and loss of hydraulic conductance (Tyree and Ewers 1991). This process is referred to here as plant hydraulic stress. Plant hydraulics in SPA are represented by two PFT-specific parameters, stem hydraulic conductance and stem hydraulic capacitance, which moderate leaf water potential (LWP) in each layer depending on soil water potential, leaf layer transpiration rate and hydraulic head (i.e. gravitational potential). Stem hydraulic conductance determines the rate of xylem flow, which transports water from soil to leaf through the bole and branches of the tree, while stem hydraulic capacitance determines the amount of water retention in the xylem. Stomatal conductance is calculated to optimize water use efficiency (a PFT-specific constant), subject to the constraint that LWP exceeds a defined minimum, also a PFT-specific constant (Bonan et al.

294 2014). Doing so alters the coupling between stomatal conductance and soil moisture by adding a
295 plant hydraulic mechanism between soil water and water stress in the leaf layer, which is linked
296 to LWP instead of directly to soil moisture.

297 Two configurations of the multilayer model are used in this study to parse the effects of
298 the alternative stomatal conductance and plant hydraulics representations. The first version,
299 CLM-ml-BB, is comparable to CLM4.5 as it uses Ball-Berry stomatal conductance and the soil
300 moisture stress (β_t) is applied equally to all leaf layers, though it uses the different turbulence and
301 energy closure methods mentioned above. The second version, CLM-ml-SPA, uses the SPA
302 model wherein soil moisture stress varies vertically because plant hydraulics modulate between
303 soil water potential and leaf water potential at each leaf layer. While both configurations of the
304 model include the multilayer resolution of canopy physics, the effects of vertically varying water
305 stress are unique to CLM-ml-SPA. The plant hydraulics in CLM-ml-SPA may change the
306 susceptibility of photosynthesis to canopy microclimate by linking water stress to within-canopy
307 microclimate, i.e. by applying plant hydraulic stress (i.e. closure of stomata) to leaves that have
308 lost moisture by radiation-transpiration coupling.

309 Because CLM-ml is currently an offline model formulation, it is not fully coupled to all
310 CLM processes. In the simulations presented here, CLM-ml soil water content is decoupled from
311 precipitation and evapotranspiration, requiring prescribed soil moisture input and limiting
312 simulations to shorter (~monthly) timescales. CLM-ml simulations are therefore run with
313 volumetric soil water content (SWC) and β_t prescribed from the CLM4.5 simulations described
314 in Section 2.2.1 and are run for the month of July (peak growing season), only. These
315 simulations are run in offline, single point mode for the same years as the CLM4.5 simulations,
316 and are driven by the same FLUXNET atmospheric forcing, also with constant CO₂ (360 ppm).
317 The results of these simulations, along with the CLM4.5 simulations, are discussed in Sections
318 3.1-3.3.

319

320 *2.2.3 CLM5 and big-leaf plant hydraulics*

321 The most recent implementation of CLM is version 5 (CLM5), which includes new
322 hydrology, plant hydraulic stress (PHS), and the Medlyn stomatal conductance scheme (Medlyn
323 et al. 2011; Kennedy et al. 2019). The model, similar to SPA, links stomatal conductance to plant
324 water stress by mediating soil water content and transpiration via a plant hydraulics scheme that

325 maintains continuity of water mass throughout the soil-plant-atmosphere system, except the
326 canopy is modeled by a big-leaf representation that is divided into sun and shaded portions,
327 similar to CLM4.5. There are several distinctions to note between CLM5 PHS and the CLM-ml-
328 SPA model that do not allow direct comparisons of their implementation of plant hydraulic stress
329 (in addition to the differing canopy physics). For one, plant hydraulic status (i.e. leaf water
330 potential in the models) is linked directly to stomatal closure in SPA, while in CLM5 PHS a
331 *plant* water stress parameter (f_w) is calculated as a sigmoidal function parameterized by threshold
332 leaf water potential corresponding to 50% hydraulic conductance and applied in the Medlyn
333 equation for stomatal conductance (similar to β_t in CLM4.5). Secondly, SPA includes hydraulic
334 capacitance, which represents water storage in the plant hydraulic system, while CLM5 PHS
335 does not. Thirdly, the iterative process by which stomatal conductance is calculated differs
336 between SPA and CLM5.

337 Despite these differences, we can infer whether plant hydraulics affect GPP in a big-leaf
338 representation by comparing two configurations of CLM5 with different settings: i) PHS turned
339 *on* (CLM5-PHS) and ii) PHS turned *off* (CLM5-noPHS). When CLM5 is run with PHS turned
340 off, the stomatal conductance parameterization is Ball-Berry and water stress is implemented as
341 in CLM4.5 with a soil moisture stress factor, β_t , which comes directly from the soil water content
342 as opposed to the plant water stress parameter f_w used with PHS turned on. We note that even
343 though these simulations also differ in stomatal conductance parameterization (Medlyn versus
344 Ball-Berry), additional simulations (not shown) showed that the choice of stomatal conductance
345 parameterization had a small impact on simulated July GPP compared to turning plant hydraulics
346 on and off. Simulations of CLM5 using each of the two configurations are run at each
347 FLUXNET site similar to the CLM4.5 and CLM-ml runs described above, and the resulting IAV
348 in GPP simulated by these model runs is analyzed with respect to the observations and other
349 models. The CLM5 results are discussed in Section 3.5.

350

351 ***2.3 Analysis of inter-annual variability***

352 We analyze IAV in the month of July, which represents peak growing season and
353 identifies GPP responses to the direct effects of local climate variability. Although the
354 FLUXNET observations of July GPP IAV might reflect lagged responses to climate IAV earlier
355 in the growing season because of phenological responses to climate (Desai 2010), the model as

356 described above has a fixed phenological cycle and will only reflect lagged responses of GPP via
 357 lagged responses of soil moisture to prior months' climate. Otherwise, the model is representing
 358 GPP responses to July climate variability only. IAV is defined here as the annual anomaly of
 359 July GPP from the mean of July GPP over all simulated years. We define the magnitude of July
 360 IAV as the standard deviation of the July anomalies from the long-term trend (S_{IAV}),

361

$$362 \quad S_{IAV} = \frac{\sqrt{\sum_{i=1}^N (y_i - y_{i,fit})^2}}{N-1}. \quad (1)$$

363

364 Here, y_i is the annual July value (mean or sum) for year i , and $y_{i,fit}$ is simple linear best fit of
 365 annual July values over a timeseries of N years. Annual July values for GPP and leaf layer gross
 366 carbon assimilation rate (a_g) are the sum of hourly carbon uptake over the month of July. For all
 367 observed climatic driving variables (air temperature; relative humidity, and incoming SW
 368 radiation, as well as SWC (i.e. soil moisture)) simulated by CLM4.5, y_i is the July mean only
 369 including timestamps when GPP > 0. In addition to soil moisture, which for CLM4.5 and CLM-
 370 ml is simulated by CLM4.5, and also simulated in CLM5, IAV in observed precipitation
 371 accumulated from March-July (which correlates well with simulated SWC, Table 2) is calculated
 372 for additional insight.

373 The year-to-year pattern of variability is quantified as the sample z-score of the detrended
 374 anomalies,

375

$$376 \quad y_{IAV} = \frac{y_i - y_{i,fit}}{S_{IAV}} \times 100 \quad (2)$$

377

378 where y_{IAV} is the annual July anomaly relative to S_{IAV} in units of percent. A z-score of 100%
 379 indicates a positive anomaly equal to one standard deviation from the mean. Using a z-score
 380 allows the patterns of IAV in carbon flux and driving climate variables to be represented as
 381 anomalies relative to the *magnitude of variability* (i.e. S_{IAV}), and thus for variables to be
 382 compared directly, independent of their units or magnitude. Note that, because the data for one or
 383 another variable may not be normally distributed, the z-score as utilized here is *not*
 384 representative of how close a data point is to the most likely values. To determine the response of
 385 GPP to climate IAV, a simple linear regression analysis is performed by regressing y_{IAV} of

386 whole-canopy GPP (CLM4.5, CLM-ml & observations) with y_{IAV} of climatic drivers as
387 independent variables. Regressions are also performed between a_g at individual leaf layers
388 (CLM-ml, only) and climatic drivers to determine if there is a vertically-varied response of
389 carbon uptake to inter-annual climate variability. Finally, all of the climatic variables are
390 regressed with one another to determine the linear covariance between drivers. Stepwise multiple
391 linear regressions were also calculated for GPP and a_g IAV using the four drivers as possible
392 independent variables (not shown); however, the results for the multiple linear
393 regression analysis (i.e. the significant drivers it identified) were similar to the simple linear
394 regression, so we show the simple linear regression only for clarity.

395 In CLM-ml, the top of the canopy is represented by a height, h . Therefore, all multilayer
396 results displayed as a function of height are presented using relative height within the canopy, or
397 z/h , where height varies from 0 (ground) to 1 (canopy top, h).

398

399 **2.4 Simulating diffuse light effects on GPP in CLM-ml**

400 We additionally evaluate the partitioning of diffuse versus direct light in CLM to
401 determine whether canopy complexity influences the sensitivity of carbon uptake to radiation.
402 The radiation scheme in offline CLM equally partitions SW radiation into visible and near-
403 infrared energy. The visible and near-infrared bands are further partitioned into direct and diffuse
404 light using an empirical polynomial fit to the climatological diurnal cycle of surface-level
405 radiation simulated by the Community Atmosphere Model version 3 (Oleson et al. 2013). In this
406 parameterization, diffuse fraction always decreases as total visible light intensity increases, while
407 diffuse light intensity is nonlinearly related to visible intensity (Figure S2). We perform
408 additional linear regressions of gross carbon assimilation in each leaf layer (CLM-ml, only) with
409 direct and diffuse visible intensity.

410 Because the direct-diffuse partitioning parameterization is based on climatology, we test
411 the sensitivity of the multilayer model regressions to this parameterization by running
412 simulations with diffuse fraction prescribed from the available hourly PAR measurements at US-
413 UMB from 2004 to 2014. Observed diffuse fraction behaves differently as a function of total
414 radiation compared to the climatological CLM parameterization. Instead of early decline of
415 diffuse fraction at low SW irradiance like in the parameterization, observed diffuse fraction
416 remains high at lower irradiance and begins to steeply fall off at higher SW intensities (Figure

417 S3). Moreover, observed diffuse fraction depends on zenith angle (i.e. time of day), and also
418 exhibits substantial variability aside from its relationship to solar intensity and zenith angle,
419 likely due to changes in clouds and aerosols. The observed diffuse fraction tends to be higher
420 than that of the parameterization and is partly decoupled from total visible intensity. To verify
421 whether the diffuse fraction parameterization affected the simulated carbon uptake, we analyze
422 an additional simulation using the prescribed diffuse fraction. Because diffuse fraction data is
423 only available from 2004-2014, we repeat the regressions of the simulations with parameterized
424 diffuse fraction for model output from 2004-2014 only for consistency.

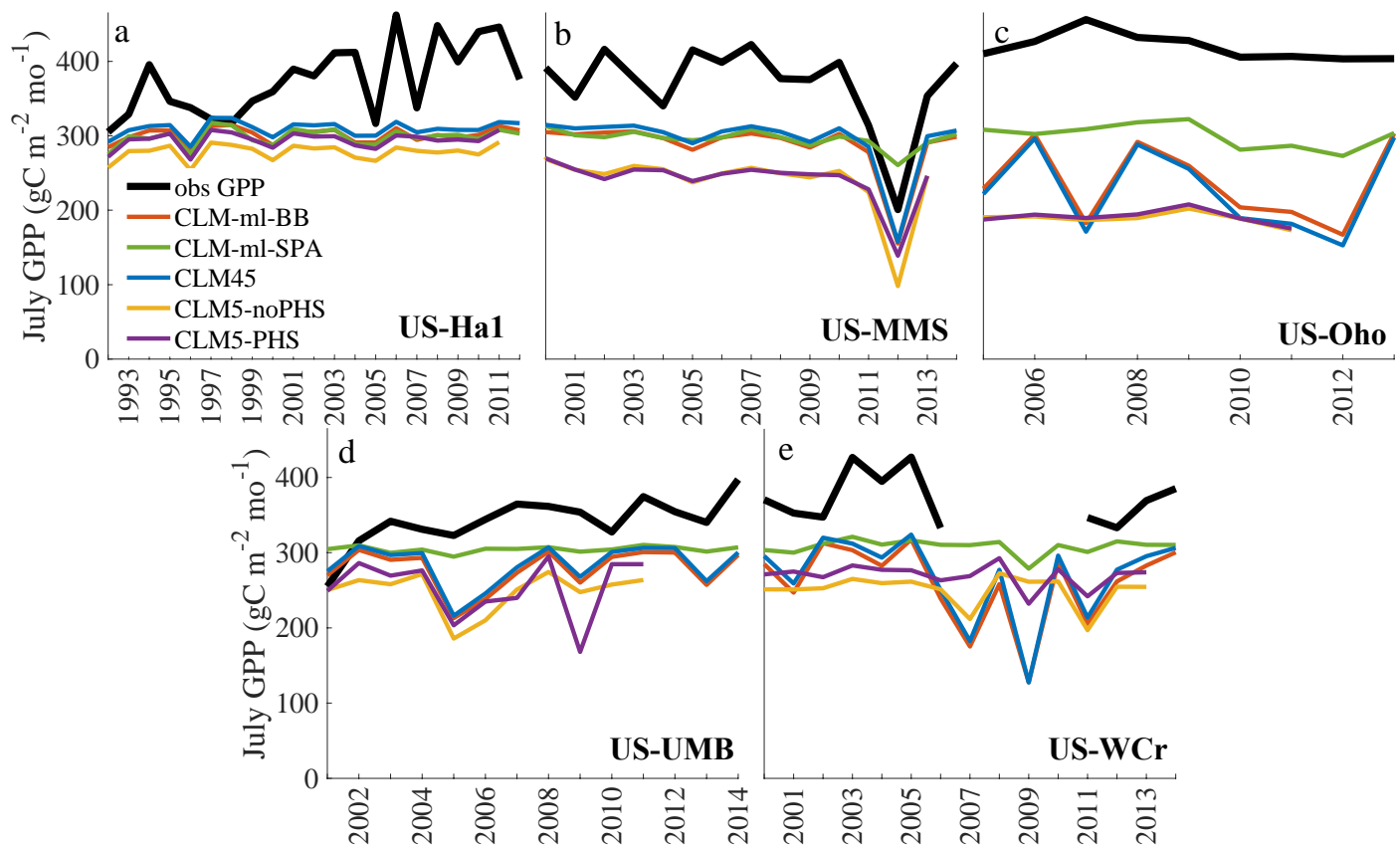
425

426 **3 Results**

427 *3.1 Canopy vertical structure in CLM-ml*

428 Vertical structure in CLM-ml manifests in vertically varying environmental conditions,
429 of which radiation primarily controls the average daytime profile of carbon assimilation rate,
430 together with leaf area density (Figure 1). At US-UMB, temperature and RH non-monotonically
431 vary throughout the canopy, where temperature has a maximum and RH, a minimum in the
432 middle of the canopy (Figures 1a,b). The exact position of these maxima varies in shorter or
433 taller canopies, but these profiles are similar for all sites based on the same leaf area distribution.
434 CLM-ml-BB is warmer and drier than CLM-ml-SPA throughout the canopy, although vertical
435 variations in temperature and RH are small at all sites (T within 0.5K and RH within 0.85%).
436 Light is extinguished exponentially from the topmost layers to the bottom (Figure 1c) in both
437 model versions. LWP, only modeled in CLM-ml-SPA, is depleted in the upper canopy where the
438 rate of photosynthesis is highest and therefore stomata are most open, coinciding with high vapor
439 pressure deficit driven by high direct insolation. Water stress is mostly limited to $z/h > 0.6$, since
440 below this level, leaves are more shaded, and LWP is maintained at roughly -0.5 MPa (Figure
441 1d). The profile of gross carbon assimilation rate per leaf area (Figure 1e, solid line) is primarily
442 controlled by APAR, and it follows the same exponential decline from top to bottom of canopy.
443 However, when the leaf area density distribution is taken into account (Figure 1e, dashed line),
444 gross carbon assimilation rate increases to a maximum near $z/h = 0.8$ and then decreases
445 exponentially to the canopy bottom. Integrated canopy GPP relies on this gross carbon
446 assimilation rate adjusted for leaf area density, and indicates that the maximum contribution in
447 the canopy to GPP is from the upper mid-canopy.

448

449 **3.2 Canopy-scale IAV of GPP and its response to climate variability**

450

451 **Figure 2.** Timeseries of mean July GPP for the FLUXNET daytime-partitioned estimate and various
 452 configurations of CLM models (see Table 1) for sites a) US-Ha1, b) US-MMS, c) US-Oho, d) US-UMB,
 453 and e) US-WCr. The US-WCr site is missing data from years 2007-2010.

454

Site	Variable	T	RH	SW	Pr	SWC ^a	GPP, obs
US-Ha1	RH	-0.17					
	Incoming SW	0.20	-0.76***				
	MAMJJ Accum. Precip.	-0.39*	0.03	0.05			
	SWC	-0.41*	0.14	-0.04	0.84***		
	GPP, obs	0.44**	-0.34	0.51**	0.15	N/A	
	GPP, CLM4.5	0.32	-0.36*	0.46**	-0.39*	-0.49**	0.27
	GPP, CLM-ml-BB	0.40*	-0.28	0.41*	-0.39*	-0.50**	0.33
	GPP, CLM-ml-SPA	0.11	-0.47**	0.57***	-0.23	-0.37*	0.26
	GPP, CLM5-PHS	0.15	-0.36	0.48**	-0.40*	-0.49**	0.18

	GPP, CLM5-noPHS	0.16	-0.35	0.49**	-0.42*	-0.55***	0.20
US-MMS	RH	-0.44*					
	Incoming SW	0.37	-0.59*				
	MAMJJ Accum. Precip.	-0.15	0.20	0.06			
	SWC	-0.68**	0.56*	-0.36	0.62		
	GPP, obs	-0.52**	0.39	0.13	0.37	0.67***	
	GPP, CLM4.5	-0.59**	0.72**	-0.12	0.44*	0.77***	0.87***
	GPP, CLM-ml-BB	-0.59**	0.72**	-0.12	0.45*	0.77***	0.87***
	GPP, CLM-ml-SPA	-0.57**	0.58**	0.06	0.26	0.54**	0.81***
	GPP, CLM5-PHS	-0.70***	0.70***	-0.09	0.47*	0.80***	0.79***
	GPP, CLM5- noPHS	-0.63**	0.69***	-0.05	0.47*	0.83***	0.82***
US-Oho	RH	-0.21					
	Incoming SW	0.32	-0.91***				
	MAMJJ Accum. Precip.	-0.27	0.47	-0.41			
	SWC	-0.30	0.73**	-0.65*	0.58		
	GPP, obs	-0.59*	-0.39	0.09	0.03	-0.10	
	GPP, CLM4.5	-0.49	0.74**	-0.67**	0.72**	0.94***	-0.01
	GPP, CLM-ml-BB	-0.47	0.75**	-0.68**	0.74**	0.94***	-0.02
	GPP, CLM-ml-SPA	-0.89***	0.25	-0.26	0.36	0.52	0.46
	GPP, CLM5-PHS	-0.86**	-0.04	-0.06	0.37	0.34	0.36
	GPP, CLM5- noPHS	-0.75*	0.06	-0.03	0.21	0.49	0.15
US-UMB	RH	-0.48*					
	Incoming SW	0.68***	-0.74***				
	MAMJJ Accum. Precip.	0.26	0.46*	-0.07			
	SWC	-0.07	0.46	-0.16	0.82***		
	GPP, obs	-0.02	0.23	0.12	0.22	0.33	
	GPP, CLM4.5	-0.11	0.52*	-0.21	0.86***	0.82**	0.25
	GPP, CLM-ml-BB	-0.10	0.52*	-0.20	0.87***	0.82**	0.26
	GPP, CLM-ml-SPA	0.18	0.34	0.09	0.70***	0.43	0.25
	GPP, CLM5-PHS	0.32	0.49	-0.10	0.89***	0.80***	0.05
	GPP, CLM5- noPHS	-0.39	0.63**	-0.43	0.75***	0.73***	0.11
US-WCr	RH	0.26					
	Incoming SW	0.65**	0.43				
	MAMJJ Accum. Precip.	0.25	-0.04	0.56**			
	SWC	0.21	0.36	0.67***	0.74***		
	GPP, obs	-0.64**	0.40	-0.17	-0.04	-0.03	

GPP, CLM4.5	0.33	0.25	0.68***	0.74***	0.86***	0.61**
GPP, CLM-ml-BB	0.30	0.28	0.69***	0.75***	0.89***	0.64**
GPP, CLM-ml-SPA	0.46*	0.31	0.44	0.47	0.56**	0.54**
GPP, CLM5-PHS	0.17	-0.05	0.20	0.45	0.47*	0.50
GPP, CLM5- noPHS	-0.26	-0.13	0.17	0.46	0.54	0.35

Table 2. Coefficient of correlation for canopy-scale linear regressions of z_{IAV} . Green shaded cells are covariances of drivers, while blue shaded cells are correlations of GPP with drivers. White numerical cells in the rightmost column are correlations of modeled GPP with observed GPP.

*** $p < 0.01$, ** $p < 0.05$, * $p < 0.10$.

^a Observed GPP was regressed with observed SWC. CLM4.5 and CLM-ml GPP were regressed with CLM4.5-simulated SWC. CLM5-PHS and CLM5-noPHS were simulated with their own respective simulated SWC.

The response of observed July GPP to climate variability at each site generally depends on the climatic driver(s) with the most pronounced IAV (Tables 2, S1). US-Ha1 is the most humid and cool of all the sites, and receives the least insolation on average. Despite low average values, incoming SW radiation is characterized by larger IAV than other driver variables at the site, and GPP IAV at US-Ha1 is most highly correlated with SW radiation ($r = 0.51$; Table 2). These regressions at US-Ha1 are robust even when the years of notable disturbance (see Section 2.1) are removed (Table S2). US-MMS is the warmest site, receives the most precipitation, and also has the highest temperature and precipitation IAV. US-MMS has the highest IAV of observed July GPP ($S_{IAV} = 55.54 \text{ gC m}^{-2} \text{ mo}^{-1}$; Table S1), and this is most highly correlated with IAV in soil moisture ($r = 0.65$; Table 2), which is mediated by evaporative demand and precipitation. GPP IAV at US-MMS is anti-correlated with temperature ($r = -0.52$; Table 2), and we note that temperature is anti-correlated with soil moisture. We note that 2012 was a drought year at US-MMS characterized by very low RH and soil moisture, which is a strong driver of the correlations at US-MMS. The linear correlation of GPP with soil moisture is substantially weakened ($r=0.29$; $p>0.10$) when the year 2012 is removed from the analysis, as is the correlation of GPP with temperature ($r=-0.21$; $p>0.10$) while the only significant correlation ($p<0.01$) becomes that of observed GPP and RH (Table S2). This suggests that outside of a drought at a relatively well-watered site like US-MMS, GPP may be far more responsive to

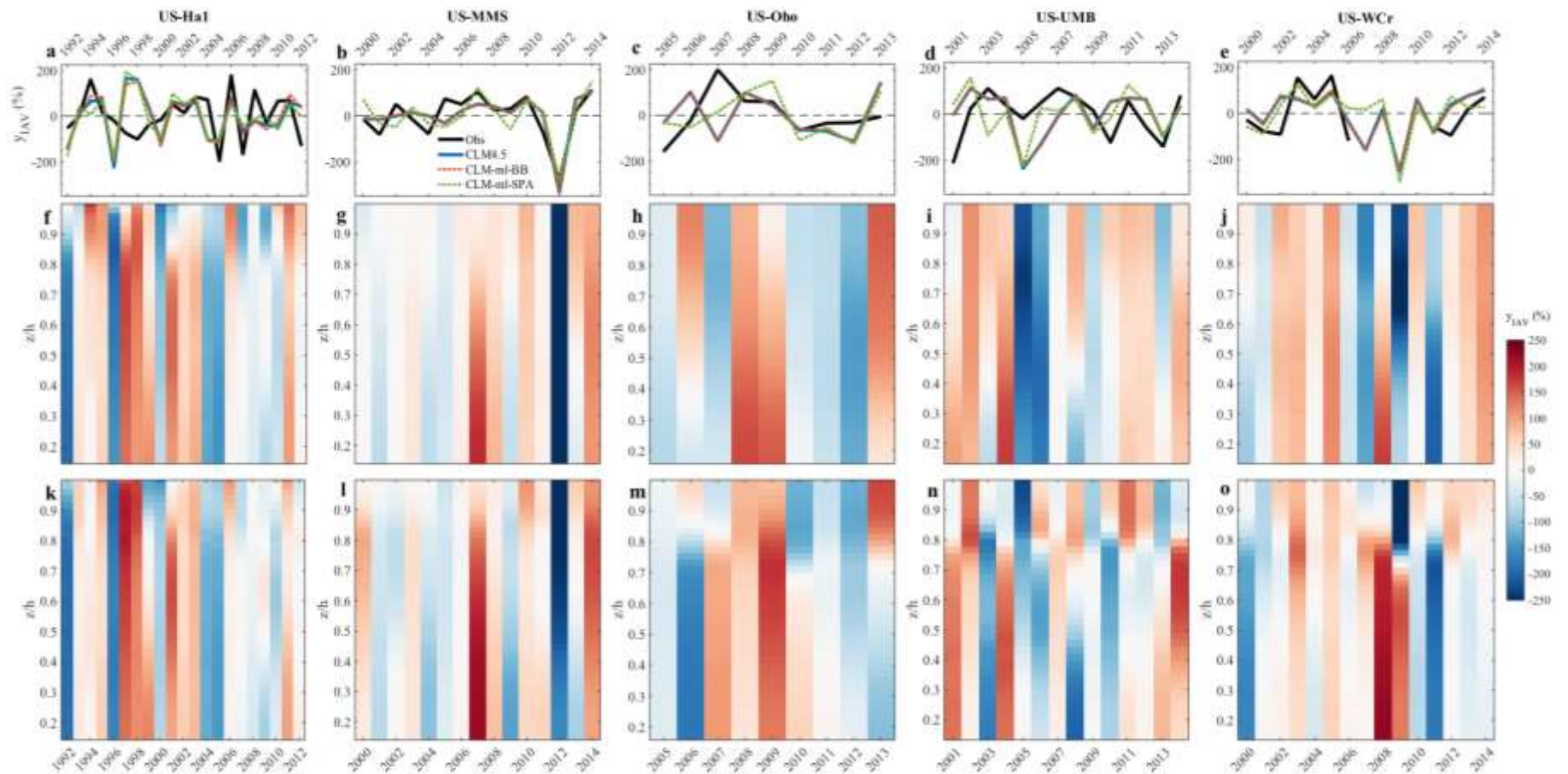
482 atmospheric conditions than soil conditions. GPP at US-Oho is the highest in magnitude, which
483 may be due to this site having the highest SW radiation, but lowest in IAV. Like US-MMS, GPP
484 at US-Oho is anti-correlated with temperature. US-UMB exhibits the lowest climate variability
485 of all of the sites, which may account for the lack of strong ($|r| > 0.5$) or significant ($p < 0.05$)
486 correlations between GPP IAV and any of the observed climate drivers given by the linear
487 regressions (Table 2). Finally, at US-WCr, GPP is anti-correlated with temperature, while
488 temperature at US-WCr has the second highest IAV among the sites. RH becomes a significant
489 driver at US-WCr, as well, when accounting for disturbance history (Table S2); otherwise, the
490 regressions remain qualitatively similar.

491 The models consistently underestimate observed July GPP at all sites by 11-46% (Figure
492 2; Table S1), which may be due to either parameter or model structural uncertainty (see Section
493 4). The simulations do, however, capture some of the observed patterns of GPP (Table 2). For
494 example, the models capture the positive correlations of GPP with incoming SW radiation and
495 temperature and negative correlation with RH at US-Ha1. They also capture the anti-correlation
496 of GPP with temperature at US-Oho. However, some of that agreement diminishes when
497 disturbance years are removed from the analysis, like at US-Ha1 (Table S2). Model-observation
498 agreement on-the-whole is fairly weak, disturbances or not, as correlations of observed GPP with
499 SWC are weak while the models still simulate a strong sensitivity of simulated GPP to SWC.
500 Therefore, the modeled GPP IAV does not correlate well with observed GPP IAV at any of these
501 sites. These results suggest that either the models overemphasize the role of soil moisture
502 variability in GPP IAV, or that there are errors between CLM4.5 simulated SWC and real-world
503 soil moisture.

504 Differences between GPP IAV simulated by CLM-ml-BB and CLM4.5 and their
505 regressions with climatic drivers are negligible for all sites (Table 2; Table S1; Figure S4),
506 implying that vertically varying microclimate and leaf area profile did not substantially impact
507 the response of GPP to climate IAV. However, the results are notably different when using SPA,
508 indicating that simulating plant hydraulics and LWP in a multi-layer model may influence the
509 IAV of GPP. CLM-ml-SPA simulations dampen July GPP IAV relative to CLM-ml-BB and
510 CLM4.5 at all sites except US-Ha1 (Table S1; Figure S4a-d). At US-Ha1, simulated July GPP
511 IAV at was slightly greater in CLM-ml-SPA than it was for CLM4.5 and CLM-ml-BB (Table
512 S1). Moreover, at all sites except US-Ha1, SPA alters the pattern of GPP IAV relative to the

513 Ball-Berry simulations, causing y_{IAV} for some years to differ by over 100% between simulations
514 (Figure 3b-e). At US-Ha1, the pattern of CLM-ml-SPA simulated July GPP IAV changes little
515 relative to that of CLM-ml-BB and CLM4.5 (Figure 3a). To explain why the multilayer model
516 only made a difference when using SPA, we analyze the individual leaf layers simulated in
517 CLM-ml in Section 3.3.

Author Manuscript



518

519

520

521

522

Figure 3. y_{IaV} for **a-e)** GPP at the canopy scale, **f-j)** carbon assimilation rate at each leaf layer in CLM-ml-BB, and **k-o)** carbon assimilation rate at each leaf layer in CLM-ml-SPA. Note the different years for each site. z/h is relative height within canopy of height h .

523 **3.3 IAV of gross carbon uptake and response to climate variability in individual leaf layers**

524 In the multilayer model simulations, IAV of gross carbon assimilation rate (a_g) differs
525 among individual leaf layers (Figure 3f-o), indicating that each layer can respond
526 independently to climate IAV. This is most apparent in the CLM-ml-SPA simulations, where
527 vertical gradients in a_g IAV are very strong. Moreover, at some layers the sign may be
528 opposite to that of other layers and even the canopy integrated GPP (Figure 3a-e), indicating
529 that the climate-driven anomalies at some layers oppose the anomalies at other layers in the
530 same year. In fact, these vertical gradients are explained by a vertically varying response to
531 climate variability (i.e. different dominant drivers at each layer), as measured by the
532 correlations between y_{IAV} of gross carbon assimilation rate (a_g) at individual canopy layers
533 with the y_{IAV} of four climate drivers (Fig. 4). To elucidate how either multilayer
534 parameterization, CLM-ml-BB or CLM-ml-SPA, affects these results, we analyze Figures 3
535 and 4 in the context of each simulation across all five sites.

536 In the CLM-ml-BB simulations, vertical gradients in a_g IAV are most apparent at US-
537 Ha1 within the upper part of the canopy (Figure 3f), with vertical gradients present at all sites
538 we simulated (Figure 3g-j). For CLM-ml-BB simulations, the sign of the a_g anomaly at each
539 layer is fairly uniform throughout the canopy, with some exceptions where there are sign
540 changes in the mid and lower canopy (e.g. 2003 and 2008 at US-UMB, Figure 3i; 2000 at
541 US-WCr, Figure 3j). For most years, the sign of the anomaly in each canopy layer
542 corresponds to the sign of the integrated GPP IAV time series for CLM-ml-BB in Figure 3a-
543 e. At all sites except US-Ha1, soil moisture was the main limiting climate variable
544 throughout the canopy, shown by the significant ($p < 0.05$), positive correlation coefficients
545 in the linear regressions at most layers (Figure 4b-e). This relatively consistent soil moisture
546 response throughout the canopy explains why GPP IAV is so similar between CLM-ml-BB
547 and CLM4.5. The sign of the correlations changes within the canopy in the CLM-ml-BB
548 simulations at some sites (excluding US-Ha1) because of the increasing dependence of a_g on
549 radiation, in tandem with incoming shortwave radiation anomalies that have the opposite
550 impact on a_g of soil moisture. For example, in years 2003 and 2008 at US-UMB (Figure 3i),
551 negative radiation anomalies (Figure S4d) drove negative a_g anomalies at $z/h < 0.4$, while
552 positive SWC anomalies drove positive a_g anomalies at $z/h > 0.4$, resulting in positive
553 anomalies in canopy-integrated GPP. Of the five deciduous sites evaluated, US-Ha1 exhibits

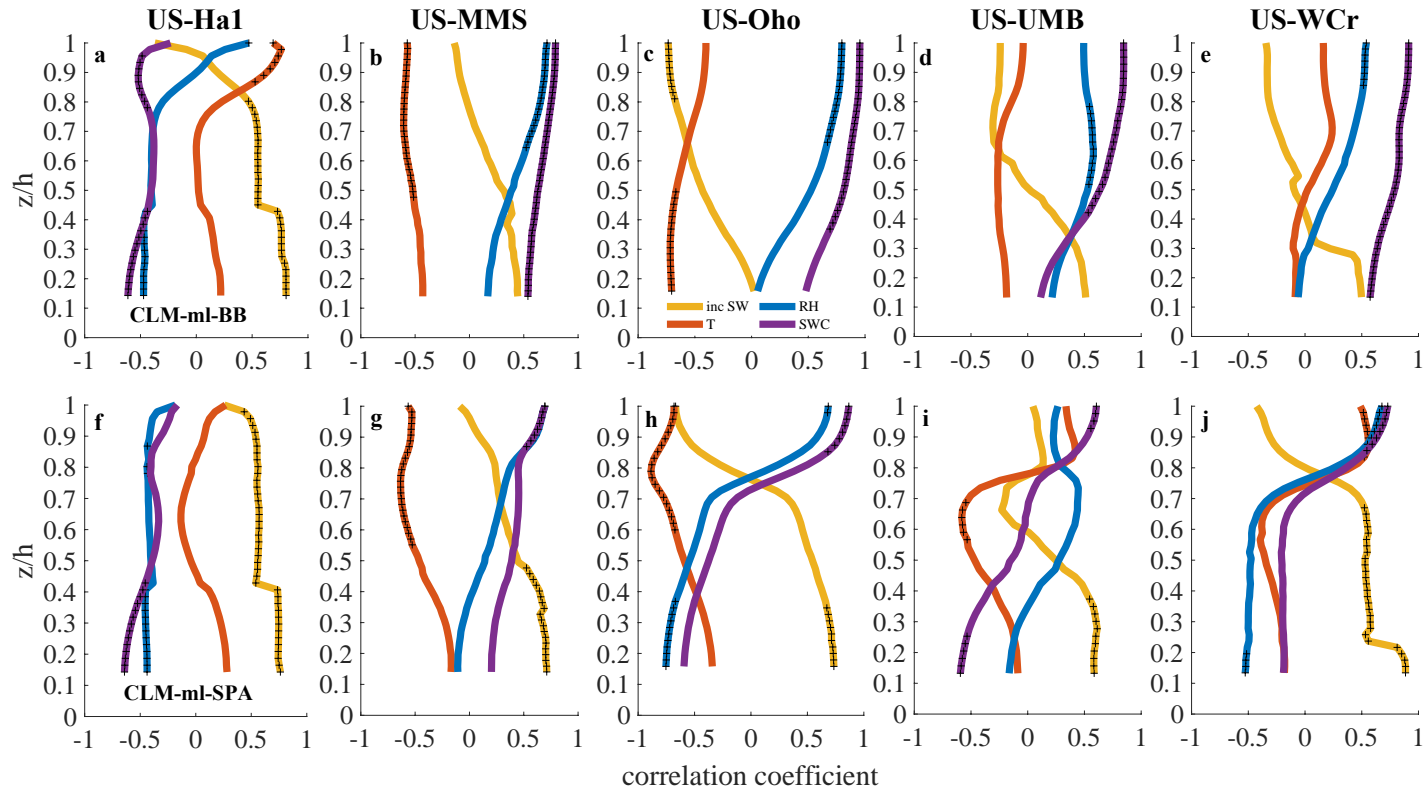
554 different behavior with CLM-ml-BB and is mainly limited by radiation (Figure 4a). The
555 transition from temperature-limited carbon uptake to radiation-limited carbon uptake at
556 around $z/h \sim 0.84$ caused strong vertical variation in leaf layer a_g IAV near that height
557 (Figure 3f). However, radiation was still the main driver throughout the canopy, which
558 accounts for the similarities between CLM-ml-BB and CLM4.5 simulations at this site.

559
560
561
562
563
564
565
566
567
568
569
570
571
572
573
574
575
576
577
578
579
580

Author Manuscript

581

582



583

584

585

Figure 4. Correlation coefficients between $y_{I,AV}$ of carbon assimilation rate at each leaf layer and $y_{I,AV}$ of the climate drivers in CLM-ml-BB (a-e) and CLM-ml-SPA (f-j). Stippled (+) points represent $p < 0.05$. z/h is relative height within canopy of height h .

586

587

588

589

590

591

592

593

594

Other climatic drivers that have significant correlations in the CLM-ml-BB simulations can be explained via their covariation with the main driving climate variable (SWC or radiation) at any site. The negative trends of carbon uptake with SWC and RH at US-Ha1 (Figure 4a) likely stem from their opposing relationship with radiation (Figure 2a). Temperature is significantly negatively correlated with carbon uptake at US-MMS in $z/h > 0.45$ (Figure 4b), but this may arise from an anti-correlation between temperature and SWC at US-MMS (Table 2). Likewise, at US-Oho radiation is strongly anti-correlated, and temperature weakly anti-correlated, with SWC and RH.

595

596

597

598

599

600

601

602

603

604

605

606

607

608

609

610

611

612

613

614

615

616

In contrast, the CLM-ml-SPA simulations show stronger vertical gradients and there are frequently sign changes within the canopy, especially at US-UMB. The vertically varying water stress in CLM-ml-SPA is predominantly why it produces qualitatively and quantitatively different regression coefficients at each layer compared to those from CLM-ml-BB, mainly at soil moisture-limited sites (Figure 4g-j). In CLM-ml-SPA, soil moisture dependence is limited to the uppermost leaf layers, which results in other climatic variables driving IAV in photosynthesis lower in the canopy. At US-MMS, US-UMB and US-Oho, there are 3 different regimes of photosynthetic response to climate variability: the upper canopy is mainly limited by soil moisture, the middle, by temperature, and the lower, by radiation (Figure 4g,h,i). At US-WCr, there are only two vertical regimes – one driven by a combination of SWC, RH and temperature at the top, and one dominated by radiation at the bottom (Figure 4j). Different drivers at different layers result in the transitions between positive and negative IAV among the leaf layers (Figure 3l-o). This occurs because since some years have anomalies in one climatic driver that oppositely affect carbon uptake compared to the effect of another climatic driver. A clear example is at US-UMB in year 2011, when high radiation and relatively higher SWC caused positive anomalies at the top and bottom of canopy, while high temperature caused a negative anomaly in the middle of the canopy (Figure 3n; Figure 2d). Many of the site-years characterized by sign changes within the canopy were associated with damped GPP IAV in CLM-ml-SPA relative to CLM-ml-BB, as is evident for example at US-Oho in 2006 and 2007 (Figure 3c,m), or at US-UMB in 2004 and 2006 (Figure 3d,n). In fact, damped response to soil moisture can also explain why CLM-ml-SPA would predict in one year a canopy-integrated GPP anomaly of opposite sign to that predicted by CLM-ml-BB. For example, at US-UMB in 2003, a year with positive soil

617 moisture anomaly and negative radiation and humidity anomalies (Figure S4d), CLM-ml-BB
618 predicted a positive anomaly in GPP due mainly to positive a_g anomalies in the upper two-thirds
619 of the canopy while CLM-ml-SPA predicted a negative GPP anomaly mainly due to the lower
620 three-quarters of the canopy (Figure 3d). In this example, CLM-ml-BB was responding to the
621 positive soil moisture anomaly, while CLM-ml-SPA with a damped soil moisture dependence
622 was responding more to the negative radiation and humidity anomalies. In contrast to soil-
623 moisture-limited sites, at US-Ha1 where radiation was the dominant driver, the layer-by-layer
624 correlations are similar to those of the CLM-ml-BB simulation (Figure 4f), and the patterns of
625 IAV in the multilayer canopy are also similar (Figure 3f,k), further suggesting that SPA has a
626 stronger impact on GPP at soil moisture limited sites.

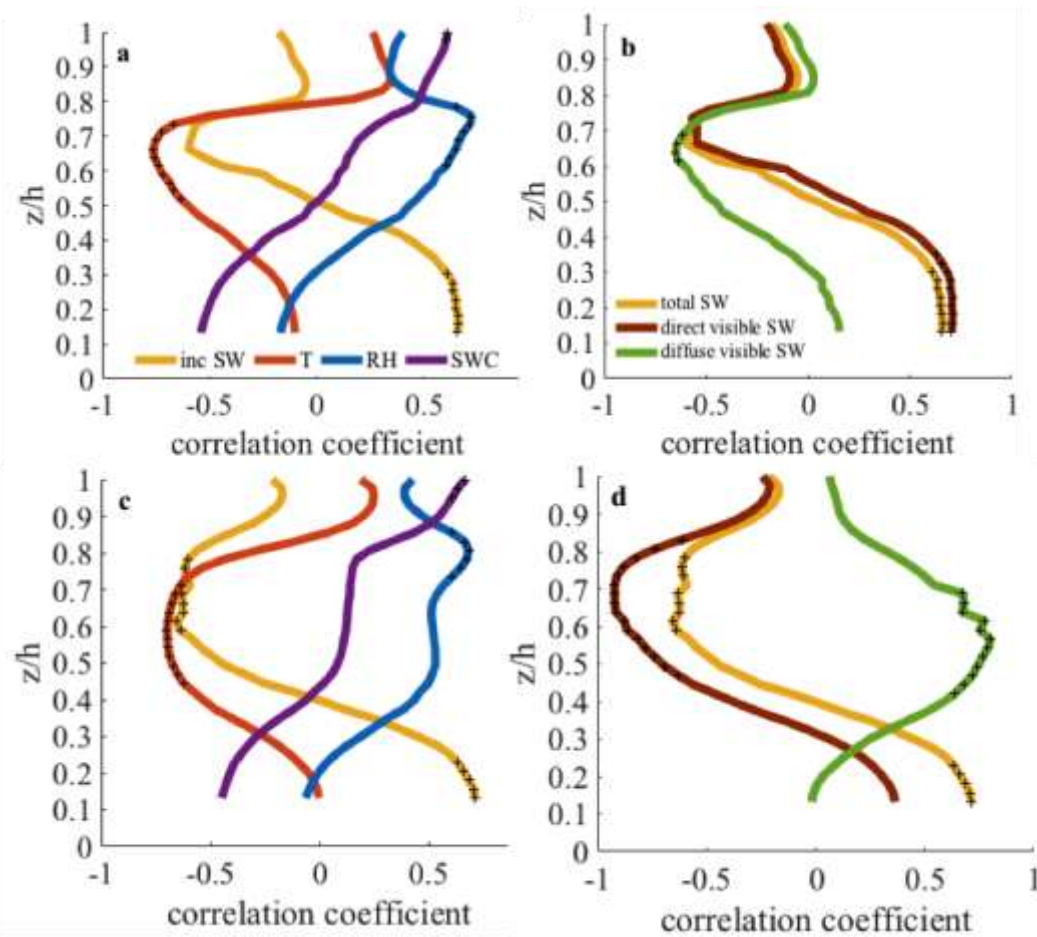
627

628 **3.4 Diffuse light effect on GPP**

629 The results presented in Section 3.3 suggest that multilayer canopy structure may affect
630 the response of GPP IAV to climate variability when plant hydraulic stress is vertically resolved,
631 exposing radiation limitation in the lower part of the canopy that was overshadowed by soil
632 moisture limitation in traditional schemes (Figure 4f-j). We therefore test whether the GPP IAV
633 is sensitive to the diffuse parameterization used in the model because these lower canopy layers
634 receive mostly diffuse light. Previous studies have shown that increased diffuse light fraction
635 increases GPP (Gu et al. 2003; Niyogi et al. 2004), although other studies suggest this effect is
636 weak in forests (Cheng et al., 2015). Simulations using prescribed diffuse fraction from
637 measured PAR at US-UMB reveal that variations in radiation were an important driver of GPP
638 IAV at $z/h = 0.6-0.8$ (Figure 5c), whereas the radiation trends at these leaf layers were not
639 significant when diffuse fraction was parameterized (Figure 5a). Diffuse evaluations at other
640 sites were not possible due to the lack of historical diffuse radiation measurements.

641 Regressions with the direct and diffuse components of the visible spectrum show that the
642 increased dependence of a_g on diffuse radiation in the middle layers of the canopy is cause for
643 the increased dependence on total SW radiation. Diffuse light positively drives a_g in the mid-
644 canopy in simulations with prescribed diffuse fraction, and conversely direct visible light has a
645 negative impact on a_g , likely because it increases temperature and VPD which have a negative
646 impact on photosynthesis.

647



648
 649 **Figure 5.** Correlation coefficients (as in Figure 4) for CLM-ml-SPA simulations at US-UMB,
 650 2004-2014 using **a,b)** Parameterized diffuse visible light fraction. **c,d)** Prescribed diffuse visible
 651 light fraction.

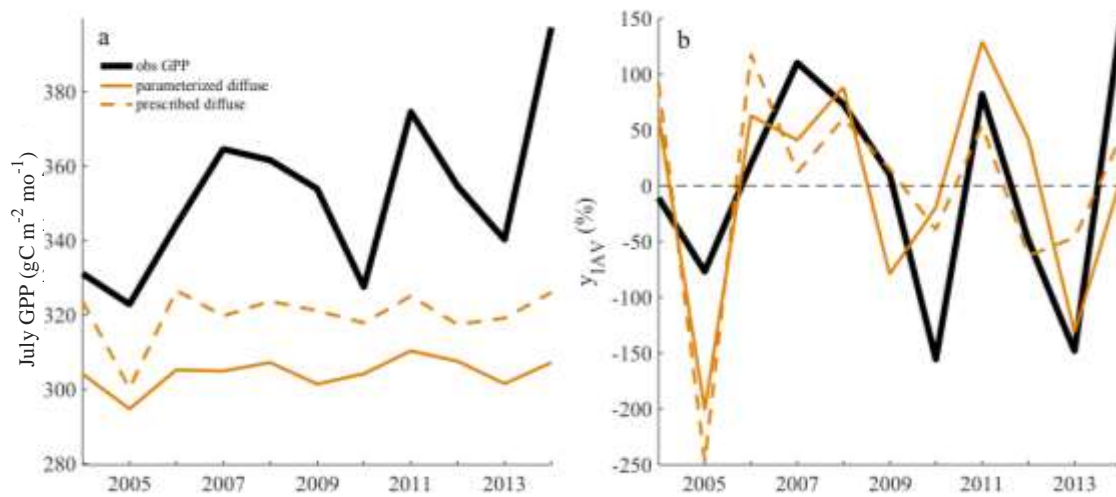
652
 653 July GPP magnitude increased for all years with prescribed diffuse fraction relative to
 654 simulations with parameterized diffuse fraction (Figure 6a). The prescribed diffuse shows some
 655 cases where it influences IAV, e.g. the large decrease in IAV from 2004-2006 (Figure 6a) but
 656 overall the impact on GPP IAV does not improve agreement with observations (Figure 6b). On
 657 hourly timescales of the light response curves, the sensitivity of GPP to diffuse fraction is
 658 different for the prescribed diffuse simulation compared to the parameterized diffuse simulation,
 659 and closer to the observed response of GPP to diffuse fraction (Figure 7). However, the positive
 660 response of GPP to diffuse fraction in CLM-ml shows a stronger gradient than observed (e.g.,
 661 higher GPP with higher diffuse fractions), indicating that the model may be overestimating the
 662 impact of diffuse light on the DBF canopy (compare Figure 7b with Figure 7c). Thus, the

663 resulting increased dependence of mid-canopy a_g should be considered with the knowledge that
 664 the model does not capture the observed diffuse light response.

665

666

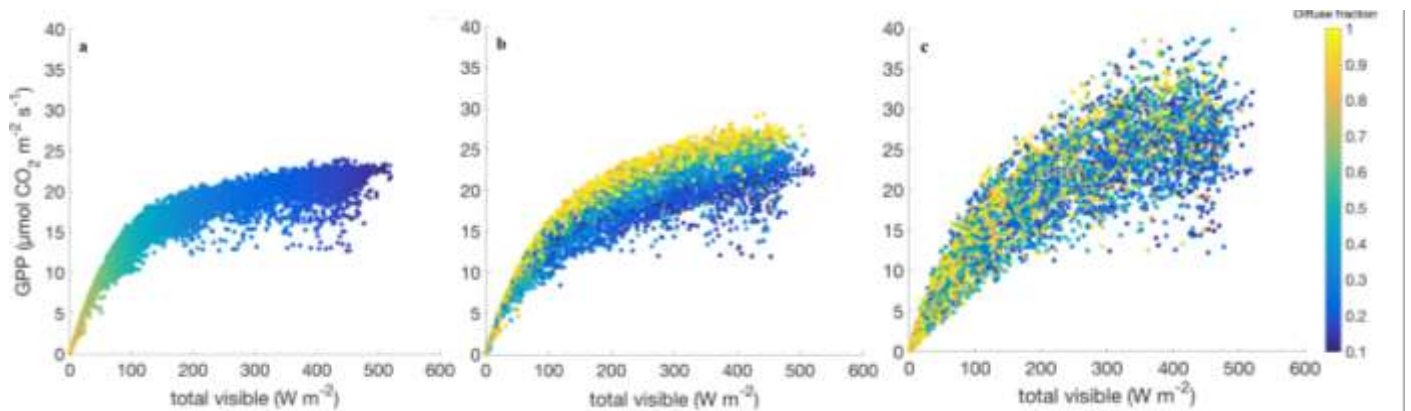
667



668

669 **Figure 6.** a) Mean July GPP and b) July GPP y_{IAV} for US-UMB comparing CLM-ml-SPA
 670 simulations using either parameterized (solid orange) or prescribed (dashed orange) diffuse
 671 fraction and observations.

672



673

674

675 **Figure 7.** For the US-UMB site (2004-2014) and the CLM-ml-SPA, the total visible light
 676 intensity (W m^{-2}) at the top of the canopy versus the hourly simulated GPP, colored by diffuse

677 light fraction (colorbar **a**) parameterized diffuse fraction and **b**) prescribed diffuse fraction.
678 Panel **(c)** shows the observed relationship based on FLUXNET data.

679

680

681 **3.5 Big-leaf plant hydraulic stress**

682 As described in Section 3.3., the use of the plant hydraulic stress parameterization in
683 CLM-ml-SPA shows that within-canopy gradients can influence the GPP response. To see
684 whether this result also applies to a big-leaf model, we compare two CLM5 simulations: one that
685 uses soil moisture stress (e.g., Ball-Berry; CLM5- noPHS) and one that uses plant hydraulic
686 stress (e.g., SPA; CLM5-PHS). The CLM5 analyses yield values of GPP S_{IAV} that are at some
687 sites more similar to CLM4.5 and CLM-ml-BB (US-Ha1, US MMS, and US-UMB), and other
688 sites more similar CLM-ml-SPA (US-Oho and US-WCr) (Figure 2; Table S1). Both CLM5-PHS
689 (PHS *on*) and CLM5-noPHS (PHS *off*) underestimate GPP magnitude more than the other
690 simulations (Figure 2; Table S1). CLM5-noPHS July mean GPP is somewhat lower than CLM5-
691 PHS, but a previous study has shown these differences to be due to the default parameters in
692 CLM for DBF and therefore not to the implementation of PHS (Franks et al. 2017). Overall, our
693 results suggest that the CLM5 simulations do not improve the simulation of GPP magnitude and
694 IAV with respect to FLUXNET observations relative to the other CLM simulations.

695 There is no clear impact of PHS in CLM5-PHS compared to CLM5-noPHS on the
696 standard deviation of July GPP (S_{IAV}). At US-MMS and US-WCr, PHS decreased S_{IAV} (from
697 35.32 to 25.85 gC m² mo⁻¹ and from 20.69 to 16.28 gC m² mo⁻¹, respectively), while at US-Oho
698 and US-UMB it increased S_{IAV} (from 7.36 to 9.2 gC m² mo⁻¹ and from 25.55 to 38.35 gC m² mo⁻¹,
699 respectively). At US-Ha1, there was negligible difference (<1 gC m² mo⁻¹). It should be noted
700 that at US-MMS, US-Oho and US-WCr, both CLM5 simulations (CLM5-PHS and CLM5-
701 noPHS) showed decreased GPP IAV relative to that of CLM4.5, suggesting that a process other
702 than PHS dampens GPP in the CLM5 model. The two CLM5 configurations are very similar
703 when evaluating the regression coefficients between GPP and climate variables (Table 2). Thus,
704 unlike the impacts of using SPA in CLM-ml instead of Ball-Berry and soil moisture stress, the
705 use of PHS in CLM5 simulations did not have a large impact on GPP variability.

706

707 **4 Discussion**

708 Single point runs at five DBF FLUXNET sites indicate that the default CLM4.5
709 underestimated both mean GPP and its IAV. Our comparison with CLM variants with more
710 complex representations of canopy structure and/or mechanistically sound representations of the
711 influence of soil moisture stress on the vegetation canopy suggests that these more sophisticated
712 model structures did not improve GPP IAV relative to observations, as will be discussed below.

713 When comparing CLM-ml-BB simulations with CLM4.5 simulations, the multilayer
714 canopy representation (including micrometeorological profiles, a leaf area profile and explicit
715 leaf layers) does not substantially impact GPP IAV or its response to inter-annual climate
716 variability relative to a big-leaf scheme. Although simulations using CLM-ml-BB show vertical
717 variation in carbon uptake, the difference in canopy-integrated GPP is negligible relative to
718 CLM4.5. The lack of substantial vertical gradients in productivity could be due in part to the
719 weak vertical microclimatic gradients in air temperature and RH in these simulations (Figure
720 1a,b). A comparison of simulated and observed air temperature and RH gradients indicates that
721 CLM-ml captures the qualities of the observed vertical variability in mean daytime temperature
722 and RH profiles at US-UMB, although it tends to underestimate its within-canopy variability of
723 air temperature by a half degree (~ 0.5 °C in the model versus 1 °C in the observations) (Figure
724 S5). Other studies have reported larger vertical micrometeorological variations of about 1-2 °C
725 (up to about 3 °C in the case of the fir) throughout aspen, fir and oak-hornbeam canopies (Elias et
726 al. 1989; Flerchinger et al. 2015), so the effects of larger micrometeorological gradients may be
727 stronger in other forest types. Another factor that could play a role in the weak vertical
728 microclimatic variations is the leaf area distribution, as the CLM-ml prescribes a beta leaf area
729 density (Figure 1e) and this may influence the microclimatic gradient. However, in a sensitivity
730 test running CLM-ml-BB with a uniform leaf area among all layers, neither GPP IAV nor its
731 regressions with climate IAV were different from simulations using the non-uniform distribution
732 (not shown). Taken together, these results suggest that the multilayer representation in CLM-ml-
733 BB does not influence the magnitude and IAV of GPP in deciduous forests compared to a big-
734 leaf model.

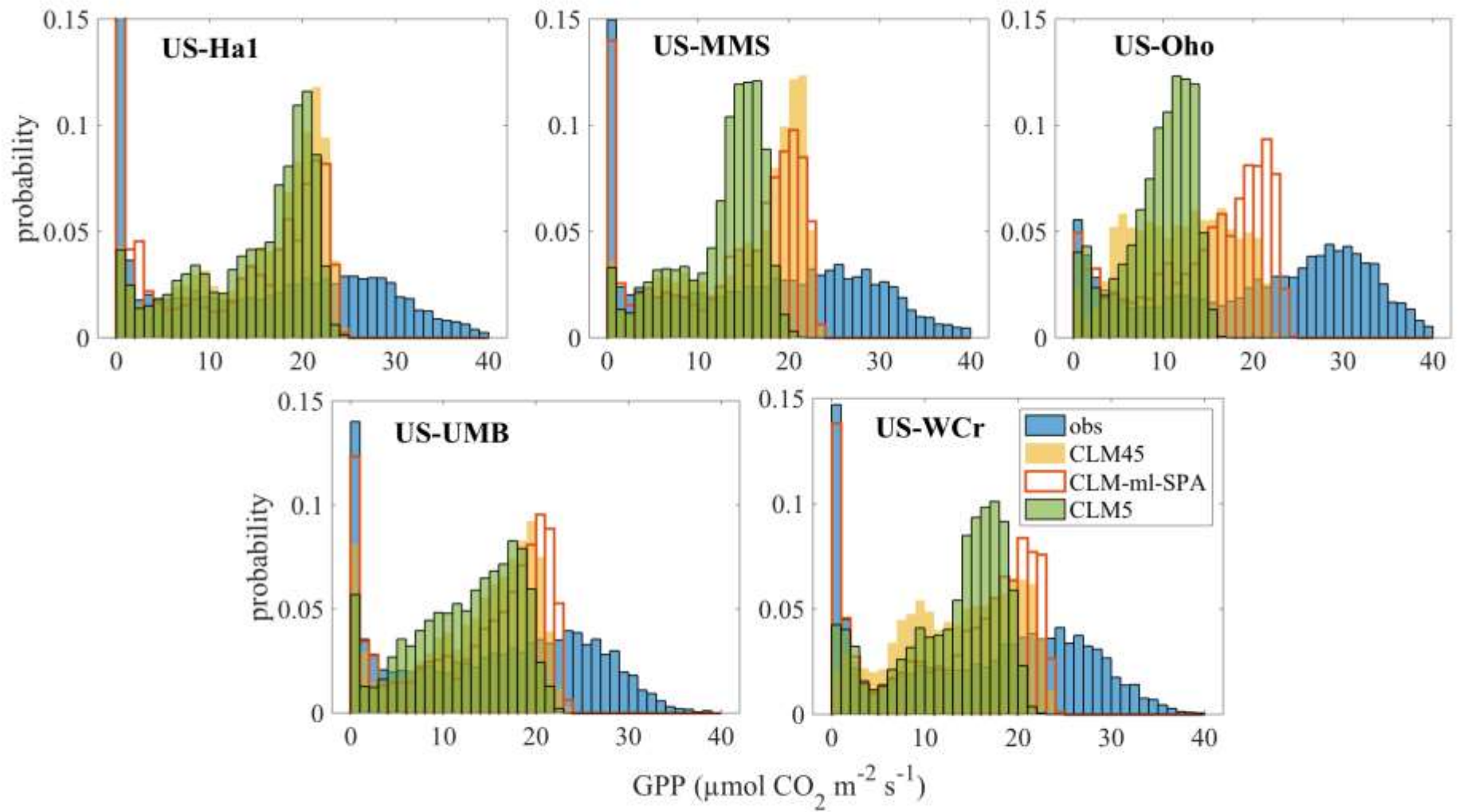
735 While the role of temperature and atmospheric water vapor within a canopy did not have
736 a strong impact, the role of leaf water and plant hydraulic stress did yield a stronger response in
737 GPP in the multi-layer model. When we replaced the Ball-Berry stomatal conductance with
738 SPA, GPP IAV was dampened compared to CLM4.5 and CLM-ml-BB, and altered the

739 relationships between carbon uptake and climate IAV. The dampened IAV is traceable to the
740 impact of plant hydraulic stress, which limits the impact of soil moisture stress to the uppermost
741 canopy layers where radiation drives high transpiration and depletes leaf water (Figure 1c,d).
742 The high transpiration rates in the upper leaf layers ($z/h > 0.6$) can only be maintained if
743 adequate soil water is available to replenish their LWP, which often results in LWP falling below
744 the threshold for stomata to remain open (-2 MPa). Meanwhile, there is less transpiration and
745 water loss at lower leaf layers ($z/h < 0.6$), allowing these layers to maintain LWP above -1 MPa
746 and to continue photosynthesizing even at low values of soil water (Figure S6). The result is that
747 the mid-canopy and lower canopy are not sensitive to soil moisture, and thus yield a negative
748 correlation with temperature and a positive correlation with radiation. As the lower canopy
749 layers decouple from soil water limitation, their sensitivity to other drivers becomes more
750 important and can result in sharp transitions in the sign of IAV within the canopy. Since these
751 transitions usually occur in the upper half of the canopy where most of the leaf area is distributed
752 (Figure 1e) and the impact on GPP is greatest, these sign transitions can result in canopy-
753 integrated IAV near zero. The representation of alternatively water limited and temperature (or
754 radiation) limited leaf layers and the cancelation between the a_g anomalies in these layers would
755 not be captured by a single leaf layer. Thus, when SPA is used, the multilayer representation of
756 the canopy significantly modifies IAV in GPP compared to the default model.

757 FLUXNET carbon fluxes (including partitioned fluxes like GPP) are subject to a ~20%
758 random error (Richardson et al. 2006), and observational GPP IAV (up to ~10-15% of the mean,
759 on average) is encompassed within that error range. Thus, the models' performance with respect
760 to observed GPP IAV should be interpreted with caution. However, with respect to mean July
761 GPP, all of the CLM variants have a negative bias relative to the observations well outside of the
762 20% error range. An analysis of hourly GPP at all sites shows that not a single model variant can
763 simulate the highest values of GPP in the hourly observations (Figure 8). A previous analysis of
764 FLUXNET data showed that hours with the highest GPP explained most of the IAV in annual
765 GPP (Zscheischler et al. 2016), and the inability of the model to capture the upper range of
766 variability may be one of the reasons why monthly-scale GPP, and possibly its IAV, were not
767 simulated accurately in this study. Our analyses in Section 3.2 also showed that disturbances at some
768 sites may have greatly impacted the regressions of GPP with climate drivers, implying that disturbances
769 are an important source of error both in the flux observations as well as in the models (given that the

770 models as configured here do not simulate disturbance events).

Author Manuscript



771

772

773

Figure 8. Histograms of daytime hourly GPP ($\text{GPP} > 0$) for FLUXNET observations and model simulations at all five study sites.

774 The representation of the interannual variability of hydrologic factors like soil moisture
775 and evapotranspiration in CLM also show biases relative to observations (Figures S7 and S8).
776 Soil moisture at all but one site (US-MMS) is either over- or underestimated, and does not
777 exhibit the same inter-annual pattern as in the observations (Figure S7). Like GPP, latent heat
778 flux is predominantly underestimated by all model versions (Figure S8). Including plant
779 hydraulics in CLM-ml and CLM5 increase mean latent heat exchange, improving some biases;
780 however, where there was little bias in latent heat exchange simulated by CLM5-noPHS (US-
781 WCr), CLM-PHS overestimated latent heat exchange. Given that evapotranspiration is inherently
782 linked to photosynthesis via stomatal opening in the model parameterizations, it is not surprising
783 that these biases persist in the water budget. According to our regressions between GPP and soil
784 moisture for the simulations and FLUXNET observations, CLM appears to overestimate the
785 influence of soil moisture on GPP IAV when using traditional soil moisture stress, which might
786 affect the timing of the positive and negative anomalies. However, it is unclear how simulated
787 soil moisture may have affected the distribution of simulated hourly GPP. Two central pieces in
788 model development leading from CLM4.5 to CLM5 were soil hydrology and plant hydraulics
789 (Kennedy et al. 2019), which, like SPA, modulates photosynthesis via plant water status rather
790 than soil water status. Using the eddy covariance observations as a constraint, our analysis
791 suggests that plant hydraulics in CLM5, as well as SPA in CLM-ml, do not improve GPP
792 variability relative to the observed range of GPP, nor do they improve simulated GPP IAV.
793 While improved vegetation and soil hydrological state and its coupling to carbon remains an
794 important model development area, future modifications to stomatal conductance and
795 photosynthesis in CLM should also address factors, or interactions among multiple factors, that
796 contribute to periods of high GPP.

797 The influence of parametric uncertainty on modeled GPP IAV and magnitude could be an
798 important component in disentangling model biases. Studies show that model parameters at
799 single sites differ from default parameters utilized in global-scale simulation of PFTs (e.g. Post et
800 al. 2018). Our study did not address the parametric uncertainty in these models at the selected
801 study sites, but instead focused on model structural differences. Additional model sensitivity
802 studies would be required to fully explore the parameter space within the CLM model versions.
803 By example, Figure S9 demonstrates the effects of varying parameter choices related to stomatal
804 conductance and plant hydraulics on simulated July GPP at US-UMB, and highlights the

805 challenges at using parameteric changes to improve the simulation of GPP IAV. Selecting
806 optimal parameters may not be straightforward or even productive, as Bonan et al. (2014)
807 showed that optimizing these parameters alone for a single site may not lead to improved model
808 representativeness given large uncertainty in optimal parameter values (see Figure 17 in Bonan
809 et al. 2014).

810 In addition to the model structural and parametric uncertainties in vegetation and soil
811 hydrology discussed above, the model-data discrepancy could be due to other canopy structural
812 factors, as well as biophysical or biochemical processes not represented in this study. For
813 example, leaf clumping (i.e. the tendency of leaves to overlap in “clumps”) and leaf angle are
814 both found to vary with height and enhance canopy response to the light environment. Several
815 modeling studies show that clumping increases canopy carbon uptake, primarily by increasing
816 intercepted radiation in shaded leaves (Baldocchi & Harley 1995; Chen et al. 2003; Walcroft et
817 al. 2005). The carbon gains from leaf clumping (versus randomly distributed leaves) is even
818 greater when the vertical heterogeneity of leaf clumping is included (Walcroft et al. 2005).
819 Another notable, vertically distributed canopy architectural trait is leaf angle, which may
820 optimize tradeoffs between radiation-induced leaf stresses and intercepted photosynthetic
821 radiation, and serve to increase carbon uptake in shaded leaves (Niinemets 1998). Perhaps these
822 architectural traits would serve to improve the models’ negative biases. Vegetation phenology
823 and pre-growing season climatological impacts, oversimplified by these models, could have
824 affected simulated GPP IAV, as observational evidence shows that the seasonal maximum GPP
825 (i.e., July GPP) in temperate forests exhibits lagged relationships to variability in spring climate
826 and bud burst phenology (Ouimette et al. 2018; Baldocchi et al. 2018). Another study shows that
827 forest stands that are older and/or exhibit higher species diversity tend to dampen IAV of net
828 carbon uptake in forests, a feature that is not simulated in CLM (Musavi et al. 2017). Finally,
829 coupled carbon-nitrogen biogeochemistry may greatly affect modeled responses of land carbon
830 exchange to climate variability (Thornton et al. 2007), which could be especially important in the
831 multilayer model setting since some deciduous forests have significant vertical variation in leaf
832 nitrogen (Ellsworth and Reich 1993).

833

834 **5 Conclusions**

835 The results of the multilayer canopy model simulations show that the influence of the

836 multilayer canopy representation on simulated GPP IAV and its response to climate variability
837 depended on the model stomatal conductance and water stress that was used. This result was
838 consistent at five DBF sites with differing climates in the Northern US. Among four soil
839 moisture-limited sites (US-MMS, US-Oho, US-UMB, US-WCr), CLM-ml simulations using
840 Ball-Berry stomatal conductance showed that soil moisture was the dominant driver at all canopy
841 layers, while radiation was the main driver at US-Ha1. Simulating vertically resolved LWP
842 profiles and plant hydraulic stress at individual leaf layers (CLM-ml-SPA) dampens total GPP
843 IAV due to a combination of the reduced impact of soil moisture and opposing leaf layer
844 anomalies at different regimes in the canopy.

845 The simulated soil moisture response at the four soil-moisture-limited sites was limited to
846 the upper canopy layers, diminishing the overall impact of soil moisture on the canopy. Other
847 drivers - temperature and radiation – take precedence in the middle and lower canopy leaf layers,
848 altering the pattern of GPP IAV and ultimately dampening it. Because radiation IAV dominated
849 the climatic influence on GPP IAV at US-Ha1, the particular moisture stress treatment (e.g.,
850 Ball-Berry or SPA) does not have an impact at this site. However, relative to FLUXNET
851 observations, CLM-ml-SPA has a larger bias with observations than models without vertically
852 resolved leaf water stress with respect to GPP IAV magnitude and y_{IAV} . Despite the realism
853 when simulating plant hydraulic stress, a multilayer canopy representation does not make gains
854 in terms of representativeness of the observations. The same GPP IAV dampening was not
855 observed between single-layer canopy simulations of CLM5 with and without plant hydraulic
856 stress, indicating that the dampening was unique to the multilayer implementation. However, it
857 cannot be certain whether the dampening in the multi-layer model was because stomatal
858 conductance in SPA is designed to optimize water use efficiency, which differs from the
859 empirical stomatal conductance in Ball-Berry, or because water stress varied by leaf layer.

860 Additionally, it was also shown that on diffuse light effects on canopy carbon uptake did
861 not improve the simulation of GPP IAV, although it did cause the mid-canopy to become more
862 sensitive to shortwave radiation. Forcing model simulations with observed diffuse fraction
863 slightly increased the magnitude of simulated carbon uptake, which is more consistent with
864 observations. However, the overall impact of diffuse light in the model was not consistent with
865 observations and model-predicted diffuse effect when prescribing observed diffuse fraction was
866 considerably overestimated relative to the observed diffuse effect. Future work is needed to

867 ensure that diffuse light impacts on canopy carbon uptake are accurately modeled with respect to
868 observations.

869 Understanding the evolution of the terrestrial carbon sink is critical to the carbon balance
870 in the atmosphere and the mitigation of anthropogenic climate change, and this study attempts to
871 use a model to delineate the response of individual terrestrial carbon processes to climate
872 variability. Our analysis shows that CLM4.5, CLM5 and CLM-ml all grossly underestimate GPP
873 at mid-latitude deciduous broadleaved forest FLUXNET sites and underestimate the GPP
874 response to climate variability. We show that increasing the complexity of the canopy structure
875 to better capture vegetation-atmosphere coupling does not ameliorate model deficiencies, nor
876 does increasing the complexity of the moisture stress function within the model. In fact, adding
877 these two changes together damps overall GPP variability as described above. Together, these
878 results suggest that adding complexity in the canopy structure is alone not sufficient to resolve
879 the fundamental biases that are present when models simulate the variability of carbon uptake,
880 especially with outstanding parametric uncertainty, and that attention to the environmental
881 drivers that influence variability is still required.

882 **Acknowledgments, Samples, and Data**

883 We would like to thank NASA Interdisciplinary Science and Terrestrial Ecology for
884 funding this work via grant # NNX17AK19G. The National Center for Atmospheric Research is
885 a major facility sponsored by the National Science Foundation under Cooperative Agreement
886 No. 1852977. We thank the FLUXNET2015 dataset contributors for acquiring, maintaining, and
887 providing data used in this study, specifically Chris Vogel at University of Michigan Biological
888 Station for providing additional meteorological data for US-UMB, as well as site PIs and data
889 managers for communicating site disturbances. We additionally thank Thiago Dos Santos for
890 providing single-point CLM5 simulations and Zachary Butterfield for editorial advice. The
891 authors declare no competing interests.

892
893 Model simulation data can be found on University of Michigan's Deep Blue data repository at:
894 <https://doi.org/10.7302/scmk-rf50>.

895 **References**

896 Ahlström, A., Raupach, M. R., Schurgers, G., Smith, B., Arneth, A., Jung, M., ... & Kato, E.
897 (2015). The dominant role of semi-arid ecosystems in the trend and variability of the land
898 CO₂ sink. *Science*, 348(6237), 895-899.

- 899 Anav, A., Friedlingstein, P., Kidston, M., Bopp, L., Ciais, P., Cox, P., ... & Zhu, Z. (2013).
 900 Evaluating the land and ocean components of the global carbon cycle in the CMIP5 Earth
 901 System Models. *Journal of Climate*, 26(18), 6801-6843.
- 902 Anav, A., Friedlingstein, P., Beer, C., Ciais, P., Harper, A., Jones, C., ... & Piao, S. (2015).
 903 Spatiotemporal patterns of terrestrial gross primary production: A review. *Reviews of*
 904 *Geophysics*, 53(3), 785-818.
- 905 Aranda, I., Cano, F. J., Gasco, A., Cochard, H., Nardini, A., Mancha, J. A., Lopez, R., &
 906 Sanchez-Gomez, D. (2015). Variation in photosynthetic performance and hydraulic
 907 architecture across European beech (*Fagus sylvatica* L.) populations supports the case for
 908 local adaptation to water stress. *Tree Physiology*, 35(1), 34–46.
 909 <https://doi.org/10.1093/treephys/tpu101>
- 910 Arora, V. K., Boer, G. J., Friedlingstein, P., Eby, M., Jones, C. D., Christian, J. R., ... & Hajima,
 911 T. (2013). Carbon–concentration and carbon–climate feedbacks in CMIP5 Earth system
 912 models. *Journal of Climate*, 26(15), 5289-5314.
- 913 Baldocchi, D. D., & Harley, P. C. (1995). Scaling carbon dioxide and water vapour exchange
 914 from leaf to canopy in a deciduous forest. II. Model testing and application. *Plant, Cell &*
 915 *Environment*, 18(10), 1157–1173. <https://doi.org/10.1111/j.1365-3040.1995.tb00626.x>
- 916 Baldocchi, D. D., Wilson, K. B., & Gu, L. (2002). How the environment, canopy structure and
 917 canopy physiological functioning influence carbon, water and energy fluxes of a
 918 temperate broad-leaved deciduous forest—an assessment with the biophysical model
 919 CANOAK. *Tree Physiology*, 22(15-16), 1065-1077.
- 920 Baldocchi, D., Chu, H., & Reichstein, M. (2018). Inter-annual variability of net and gross
 921 ecosystem carbon fluxes: A review. *Agricultural and Forest Meteorology*, 249, 520-533.
- 922 Baldocchi, D., Ryu, Y., & Keenan, T. (2016). Terrestrial carbon cycle
 923 variability. *F1000Research*, 5.
- 924 Beer, C., Reichstein, M., Tomelleri, E., Ciais, P., Jung, M., Carvalhais, N., ... & Bondeau, A.
 925 (2010). Terrestrial gross carbon dioxide uptake: global distribution and covariation with
 926 climate. *Science*, 329(5993), 834-838.
- 927 Bonan, G. B., Williams, M., Fisher, R. A., & Oleson, K. W. (2014). Modeling stomatal
 928 conductance in the earth system: linking leaf water-use efficiency and water transport
 929 along the soil–plant–atmosphere continuum. *Geoscientific Model Development*, 7(5),
 930 2193-2222.
- 931 Bonan, G. B., Patton, E. G., Harman, I. N., Oleson, K. W., Finnigan, J. J., Lu, Y., & Burakowski,
 932 E. A. (2018). Modeling canopy-induced turbulence in the Earth system: a unified
 933 parameterization of turbulent exchange within plant canopies and the roughness sublayer
 934 (CLM-ml v0). *Geoscientific Model Development*.

- 935 Bonan, G. B., & Doney, S. C. (2018). Climate, ecosystems, and planetary futures: The challenge
936 to predict life in Earth system models. *Science*, 359(6375), eaam8328.
- 937 Carlson, D. W., & Groot, A. (1997). Microclimate of clear-cut, forest interior, and small
938 openings in trembling aspen forest. *Agricultural and Forest Meteorology*, 87(4), 313-329.
- 939 Chang, K. Y., & Chen, S. H. (2018). Canopy profile sensitivity on surface layer simulations
940 evaluated by a multiple canopy layer higher order closure land surface
941 model. *Agricultural and forest meteorology*, 252, 192-207.
- 942 Chen, J., Saunders, S. C., Crow, T. R., Naiman, R. J., Broszofski, K. D., Mroz, G. D., ... &
943 Franklin, J. F. (1999). Microclimate in forest ecosystem and landscape ecology: variations
944 in local climate can be used to monitor and compare the effects of different management
945 regimes. *BioScience*, 49(4), 288-297.
- 946 Chen, J. M., Liu, J., Leblanc, S. G., Lacaze, R., & Roujean, J.-L. (2003). Multi-angular optical
947 remote sensing for assessing vegetation structure and carbon absorption. *Remote Sensing
948 of Environment*, 84(4), 516–525. [https://doi.org/10.1016/S0034-4257\(02\)00150-5](https://doi.org/10.1016/S0034-4257(02)00150-5)
- 949 Cheng, S. J., Bohrer, G., Steiner, A. L., Hollinger, D. Y., Suyker, A., Phillips, R. P., &
950 Nadelhoffer, K. J. (2015). Variations in the influence of diffuse light on gross primary
951 productivity in temperate ecosystems. *Agricultural and Forest Meteorology*, 201, 98-110.
- 952 Collatz, G. J., Ball, J. T., Grivet, C., & Berry, J. A. (1991). Physiological and environmental
953 regulation of stomatal conductance, photosynthesis and transpiration: a model that
954 includes a laminar boundary layer. *Agricultural and Forest meteorology*, 54(2-4), 107-
955 136.
- 956 De Frenne, P., Rodríguez-Sánchez, F., Coomes, D. A., Baeten, L., Verstraeten, G., Vellend, M.,
957 ... & Decocq, G. M. (2013). Microclimate moderates plant responses to macroclimate
958 warming. *Proceedings of the National Academy of Sciences*, 110(46), 18561-18565.
- 959 Desai, A. R. (2010). Climatic and phenological controls on coherent regional interannual
960 variability of carbon dioxide flux in a heterogeneous landscape. *Journal of Geophysical
961 Research: Biogeosciences*, 115(G3).
- 962 Drewry, D. T., Kumar, P., Long, S., Bernacchi, C., Liang, X. Z., & Sivapalan, M. (2010).
963 Ecohydrological responses of dense canopies to environmental variability: 1. Interplay
964 between vertical structure and photosynthetic pathway. *Journal of Geophysical Research:
965 Biogeosciences*, 115(G4).
- 966 Eliáš, P., Kratochvílová, I., Janouš, D., Marek, M., & Masarovičová, E. (1989). Stand
967 microclimate and physiological activity of tree leaves in an oak-hornbeam
968 forest. *Trees*, 3(4), 227-233.

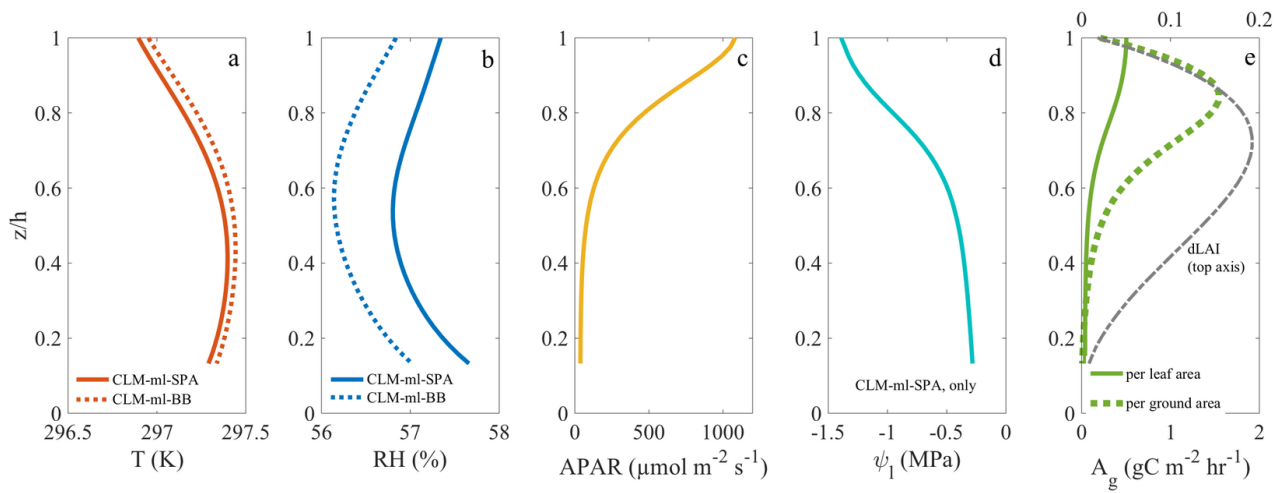
- 969 Ellsworth, D. S., & Reich, P. B. (1993). Canopy structure and vertical patterns of photosynthesis
970 and related leaf traits in a deciduous forest. *Oecologia*, *96*(2), 169-178.
- 971 Farquhar, G. D., von Caemmerer, S. V., & Berry, J. A. (1980). A biochemical model of
972 photosynthetic CO₂ assimilation in leaves of C₃ species. *Planta*, *149*(1), 78-90.
- 973 Fisher, R. A., Koven, C. D., Anderegg, W. R., Christoffersen, B. O., Dietze, M. C., Farrior, C.
974 E., ... & Lichstein, J. W. (2018). Vegetation demographics in Earth System Models: A
975 review of progress and priorities. *Global change biology*, *24*(1), 35-54.
- 976 Flerchinger, G. N., Reba, M. L., Link, T. E., & Marks, D. (2015). Modeling temperature and
977 humidity profiles within forest canopies. *Agricultural and Forest Meteorology*, *213*, 251-
978 262.
- 979 Franks, P. J., Berry, J. A., Lombardozzi, D. L., & Bonan, G. B. (2017). Stomatal function across
980 temporal and spatial scales: deep-time trends, land-atmosphere coupling and global
981 models. *Plant Physiology*, *174*(2), 583-602.
- 982 Fu, Z., Dong, J., Zhou, Y., Stoy, P. C., & Niu, S. (2017). Long term trend and interannual
983 variability of land carbon uptake—the attribution and processes. *Environmental Research
984 Letters*, *12*(1), 014018.
- 985 Funk, J. L., & Lerdau, M. T. (2004). Photosynthesis in forest canopies. *Forest canopies*, *2*, 335-
986 358.
- 987 Hellkvist, J., Richards, G., & Jarvis, P. G. (1974). Vertical gradients of water potential and tissue
988 water relations in Sitka spruce trees measured with the pressure chamber. *Journal of
989 Applied Ecology*, 637-667.
- 990 Houghton, R. A. (2000). Interannual variability in the global carbon cycle. *Journal of
991 Geophysical Research: Atmospheres*, *105*(D15), 20121-20130.
- 992 Keeling, C. D., Whorf, T. P., Wahlen, M., & Van der Plichtt, J. (1995). Interannual extremes in
993 the rate of rise of atmospheric carbon dioxide since 1980. *Nature*, *375*(6533), 666.
- 994 Keenan, T. F., Baker, I., Barr, A., Ciais, P., Davis, K., Dietze, M., ... & Hufkens, K. (2012).
995 Terrestrial biosphere model performance for inter-annual variability of land-atmosphere
996 CO₂ exchange. *Global Change Biology*, *18*(6), 1971-1987.
- 997 Kennedy, D., Swenson, S., Oleson, K. W., Lawrence, D. M., Fisher, R., Lola da Costa, A. C., &
998 Gentine, P. (2019). Implementing plant hydraulics in the community land model, version
999 5. *Journal of Advances in Modeling Earth Systems*, *11*(2), 485-513.
- 1000 Koike, T., Kitao, M., Maruyama, Y., Mori, S., & Lei, T. T. (2001). Leaf morphology and
1001 photosynthetic adjustments among deciduous broad-leaved trees within the vertical
1002 canopy profile. *Tree Physiology*, *21*(12-13), 951-958.

- 1003 Lasslop, G., Migliavacca, M., Bohrer, G., Reichstein, M., Bahn, M., Ibrom, A., ... & Wohlfahrt,
1004 G. (2012). On the choice of the driving temperature for eddy-covariance carbon dioxide
1005 flux partitioning. *Biogeosciences*, 9, 5243-5259.
- 1006 Lawrence, P. J., & Chase, T. N. (2007). Representing a new MODIS consistent land surface in
1007 the Community Land Model (CLM 3.0). *Journal of Geophysical Research:*
1008 *Biogeosciences*, 112(G1).
- 1009 Lawrence, D. M., Fisher, R. A., Koven, C. D., Oleson, K. W., Swenson, S. C., Bonan, G., ... &
1010 Kluzek, E. (2019). The Community Land Model version 5: Description of new features,
1011 benchmarking, and impact of forcing uncertainty. *Journal of Advances in Modeling Earth*
1012 *Systems*.
- 1013 Le Quéré, C., Andrew, R. M., Friedlingstein, P., Sitch, S., Pongratz, J., Manning, A. C., ... &
1014 Boden, T. A. (2017). Global carbon budget 2017. *Earth System Science Data*
1015 *Discussions*, 1-79.
- 1016 Medlyn, B. E., Duursma, R. A., Eamus, D., Ellsworth, D. S., Prentice, I. C., Barton, C. V., ... &
1017 Wingate, L. (2011). Reconciling the optimal and empirical approaches to modelling
1018 stomatal conductance. *Global Change Biology*, 17(6), 2134-2144.
- 1019 Murray, F. W. (1966). *On the computation of saturation vapor pressure* (No. P-3423). Rand
1020 Corp Santa Monica Calif.
- 1021 Musavi, T., Migliavacca, M., Reichstein, M., Kattge, J., Wirth, C., Black, T. A., ... & Varlagin,
1022 A. (2017). Stand age and species richness dampen interannual variation of ecosystem-
1023 level photosynthetic capacity. *Nature ecology & evolution*, 1(2), 0048.
- 1024 Nevison, C. D., Mahowald, N. M., Doney, S. C., Lima, I. D., Van der Werf, G. R., Randerson, J.
1025 T., ... & McKinley, G. A. (2008). Contribution of ocean, fossil fuel, land biosphere, and
1026 biomass burning carbon fluxes to seasonal and interannual variability in atmospheric
1027 CO₂. *Journal of Geophysical Research: Biogeosciences*, 113(G1).
- 1028 Niinemets, Ü. (1998). Adjustment of foliage structure and function to a canopy light gradient in
1029 two co-existing deciduous trees. Variability in leaf inclination angles in relation to petiole
1030 morphology. *Trees*, 12(7), 446-451.
- 1031 Niinemets, Ü., & Valladares, F. (2004). Photosynthetic Acclimation to Simultaneous and
1032 Interacting Environmental Stresses Along Natural Light Gradients: Optimality and
1033 Constraints. *Plant Biology*, 6(3), 254–268. <https://doi.org/10.1055/s-2004-817881>
- 1034 Norby, R. J., DeLucia, E. H., Gielen, B., Calfapietra, C., Giardina, C. P., King, J. S., ... & De
1035 Angelis, P. (2005). Forest response to elevated CO₂ is conserved across a broad range of
1036 productivity. *Proceedings of the National Academy of Sciences*, 102(50), 18052-18056.

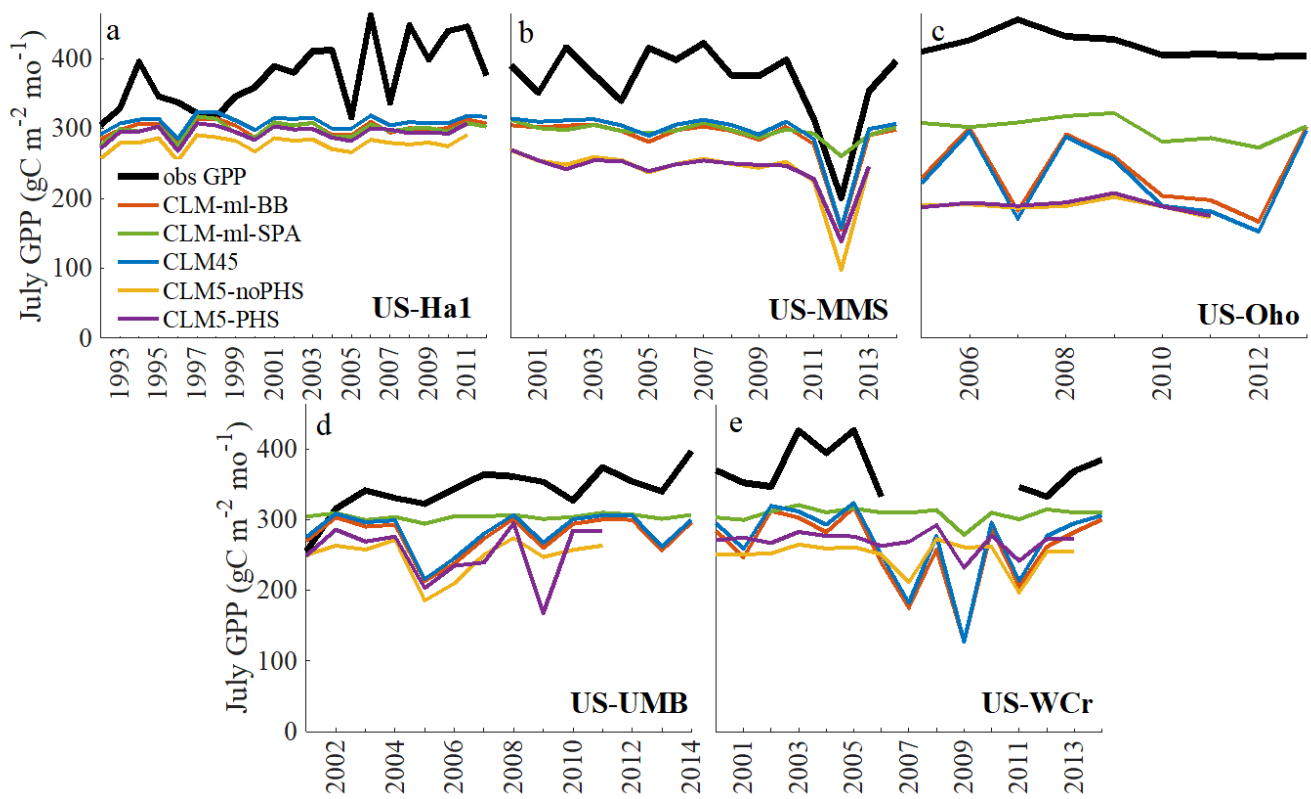
- 1037 Oleson, K. W., Lawrence, D. M., Bonan, G. B., Drewniack, B., Huang, M., Koven, C. D., ... &
1038 Swenson, S. C. (2013). Technical description of version 4.5 of the Community Land
1039 Model (CLM)(Technical Note No. NCAR/TN-503+ STR). Boulder, CO: National Center
1040 for Atmospheric Research Earth System Laboratory.
- 1041 Ouimette, A. P., Ollinger, S. V., Richardson, A. D., Hollinger, D. Y., Keenan, T. F., Lepine, L.
1042 C., & Vadeboncoeur, M. A. (2018). Carbon fluxes and interannual drivers in a temperate
1043 forest ecosystem assessed through comparison of top-down and bottom-up
1044 approaches. *Agricultural and Forest Meteorology*, 256, 420-430.
- 1045 Pan, Y., Birdsey, R. A., Fang, J., Houghton, R., Kauppi, P. E., Kurz, W. A., ... & Ciais, P.
1046 (2011). A large and persistent carbon sink in the world's forests. *Science*, 333(6045), 988-
1047 993.
- 1048 Parker, G. G., O'Neill, J. P., & Higman, D. (1989). Vertical profile and canopy organization in a
1049 mixed deciduous forest. *Vegetatio*, 85(1-2), 1-11.
- 1050 Parker, G., Tinoco-Ojanguren, C., Martínez-Yrizar, A., & Maass, M. (2005). Seasonal balance
1051 and vertical pattern of photosynthetically active radiation within canopies of a tropical dry
1052 deciduous forest ecosystem in Mexico. *Journal of Tropical Ecology*, 21(3), 283-295.
- 1053 Pastorello, G., Papale, D., Chu, H., Trotta, C., Agarwal, D., Canfora, E., ... & Torn, M. (2017).
1054 A new data set to keep a sharper eye on land-air exchanges. *Eos, Transactions American*
1055 *Geophysical Union (Online)*, 98(8).
- 1056 Post, H., Hendricks Franssen, H.-J., Han, X., Baatz, R., Montzka, C., Schmidt, M., & Vereecken,
1057 H. (2018). Evaluation and uncertainty analysis of regional-scale CLM4.5 net carbon flux
1058 estimates. *Biogeosciences*, 15(1), 187–208. <https://doi.org/10.5194/bg-15-187-2018>
- 1059 Poulter, B., Frank, D., Ciais, P., Myneni, R. B., Andela, N., Bi, J., ... & Running, S. W. (2014).
1060 Contribution of semi-arid ecosystems to interannual variability of the global carbon
1061 cycle. *Nature*, 509(7502), 600.
- 1062 Rambo, T. R., & North, M. P. (2009). Canopy microclimate response to pattern and density of
1063 thinning in a Sierra Nevada forest. *Forest ecology and management*, 257(2), 435-442.
- 1064 Richardson, A. D., Hollinger, D. Y., Burba, G. G., Davis, K. J., Flanagan, L. B., Katul, G. G., ...
1065 & Verma, S. B. (2006). A multi-site analysis of random error in tower-based
1066 measurements of carbon and energy fluxes. *Agricultural and Forest Meteorology*, 136(1-
1067 2), 1-18.
- 1068 Rödenbeck, C., Zaehle, S., Keeling, R., & Heimann, M. (2018). How does the terrestrial carbon
1069 exchange respond to inter-annual climatic variations?. *Biogeosciences*.

- 1070 Schimel, D. S., House, J. I., Hibbard, K. A., Bousquet, P., Ciais, P., Peylin, P., ... & Canadell, J.
1071 (2001). Recent patterns and mechanisms of carbon exchange by terrestrial
1072 ecosystems. *Nature*, 414(6860), 169.
- 1073 Schimel, D., Stephens, B. B., & Fisher, J. B. (2015). Effect of increasing CO₂ on the terrestrial
1074 carbon cycle. *Proceedings of the National Academy of Sciences*, 112(2), 436-441.
- 1075 Shiga, Y. P., Michalak, A. M., Fang, Y., Schaefer, K., Andrews, A. E., Huntzinger, D. H., ... &
1076 Wei, Y. (2018). Forests dominate the interannual variability of the North American carbon
1077 sink. *Environmental Research Letters*, 13(8), 084015.
- 1078 Sinclair, T. R., Murphy, C. E., & Knoerr, K. R. (1976). Development and evaluation of
1079 simplified models for simulating canopy photosynthesis and transpiration. *Journal of*
1080 *Applied Ecology*, 813-829.
- 1081 Sitch, S., Friedlingstein, P., Gruber, N., Jones, S. D., Murray-Tortarolo, G., Ahlström, A., ... &
1082 Levis, S. (2015). Recent trends and drivers of regional sources and sinks of carbon
1083 dioxide. *Biogeosciences*, 12(3), 653-679.
- 1084 Taylor, D., & Eamus, D. (2008). Coordinating leaf functional traits with branch hydraulic
1085 conductivity: Resource substitution and implications for carbon gain. *Tree Physiology*,
1086 28(8), 1169–1177. <https://doi.org/10.1093/treephys/28.8.1169>
- 1087 Thornton, P. E., Lamarque, J. F., Rosenbloom, N. A., & Mahowald, N. M. (2007). Influence of
1088 carbon-nitrogen cycle coupling on land model response to CO₂ fertilization and climate
1089 variability. *Global biogeochemical cycles*, 21(4).
- 1090 Tyree, M. T., & Ewers, F. W. (1991). The hydraulic architecture of trees and other woody
1091 plants. *New Phytologist*, 119(3), 345-360.
- 1092 von Arx, G., Dobbertin, M., & Rebetez, M. (2012). Spatio-temporal effects of forest canopy on
1093 understory microclimate in a long-term experiment in Switzerland. *Agricultural and*
1094 *Forest Meteorology*, 166, 144-155.
- 1095 Walcroft, A. S., Brown, K. J., Schuster, W. S. F., Tissue, D. T., Turnbull, M. H., Griffin, K. L.,
1096 & Whitehead, D. (2005). Radiative transfer and carbon assimilation in relation to canopy
1097 architecture, foliage area distribution and clumping in a mature temperate rainforest
1098 canopy in New Zealand. *Agricultural and Forest Meteorology*, 135(1), 326–339.
1099 <https://doi.org/10.1016/j.agrformet.2005.12.010>
- 1100 Williams, M., Richardson, A. D., Reichstein, M., Stoy, P. C., Peylin, P., Verbeeck, H., ... &
1101 Leuning, R. (2009). Improving land surface models with FLUXNET
1102 data. *Biogeosciences*, 6(7), 1341-1359.

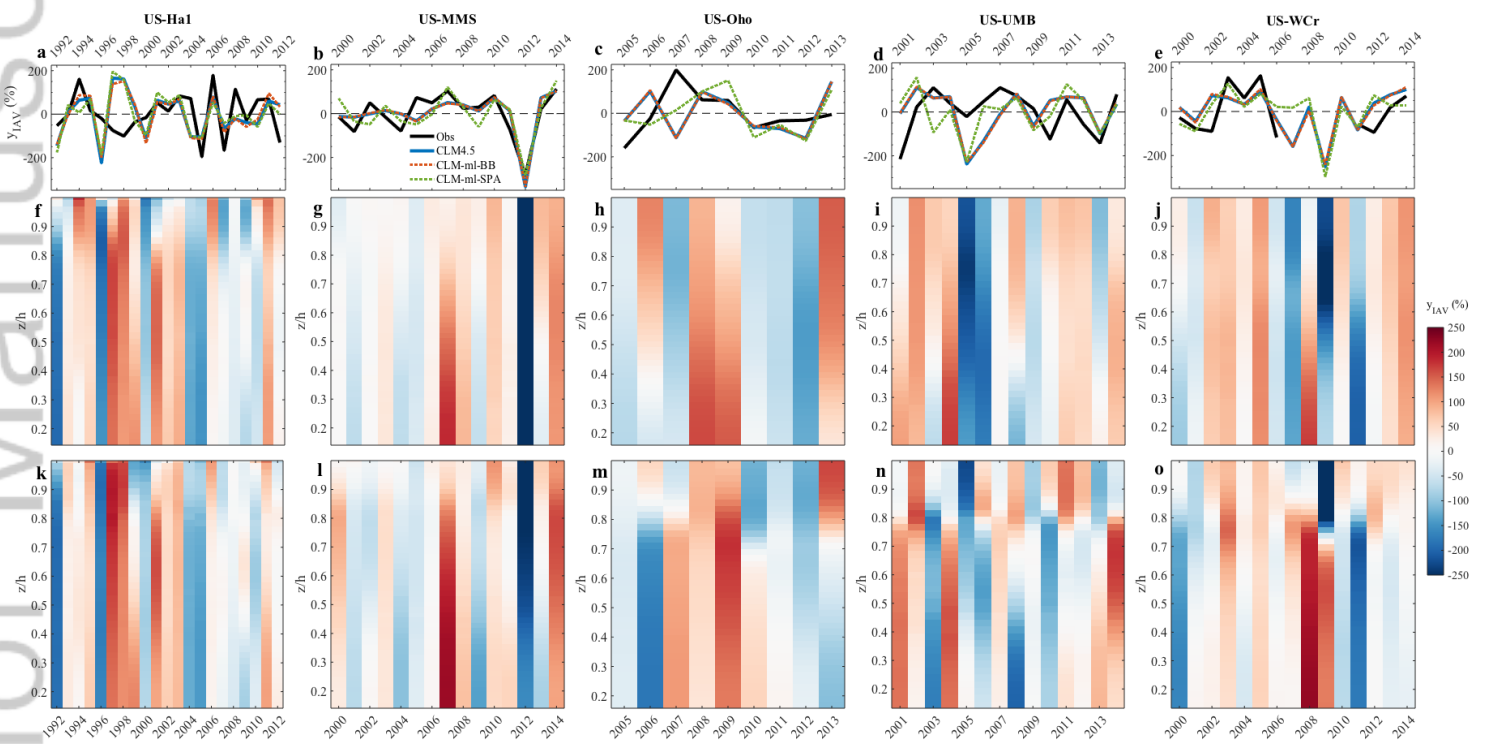
- 1103 Williams, M., Bond, B. J., & Ryan, M. G. (2001). Evaluating different soil and plant hydraulic
1104 constraints on tree function using a model and sap flow data from ponderosa pine. *Plant,*
1105 *Cell & Environment*, 24(7), 679-690.
- 1106 Williams, M., Rastetter, E. B., Fernandes, D. N., Goulden, M. L., Wofsy, S. C., Shaver, G. R., ...
1107 & Nadelhoffer, K. J. (1996). Modelling the soil-plant-atmosphere continuum in a
1108 *Quercus–Acer* stand at Harvard Forest: the regulation of stomatal conductance by light,
1109 nitrogen and soil/plant hydraulic properties. *Plant, Cell & Environment*, 19(8), 911-927.
- 1110 Wu, Y., Brashers, B., Finkelstein, P. L., & Pleim, J. E. (2003). A multilayer biochemical dry
1111 deposition model 2. Model evaluation. *Journal of Geophysical Research:*
1112 *Atmospheres*, 108(D1), ACH-2.
- 1113 Zeng, X., & Dickinson, R. E. (1998). Effect of surface sublayer on surface skin temperature and
1114 fluxes. *Journal of climate*, 11(4), 537-550.
- 1115 Zhang, J.-L., & Cao, K.-F. (2009). Stem hydraulics mediates leaf water status, carbon gain,
1116 nutrient use efficiencies and plant growth rates across dipterocarp species. *Functional*
1117 *Ecology*, 23(4), 658–667. <https://doi.org/10.1111/j.1365-2435.2009.01552.x>
- 1118 Zscheischler, J., Fatichi, S., Wolf, S., Blanken, P. D., Bohrer, G., Clark, K., ... & Seneviratne, S.
1119 I. (2016). Short-term favorable weather conditions are an important control of interannual
1120 variability in carbon and water fluxes. *Journal of Geophysical Research:*
1121 *Biogeosciences*, 121(8), 2186-2198.
1122



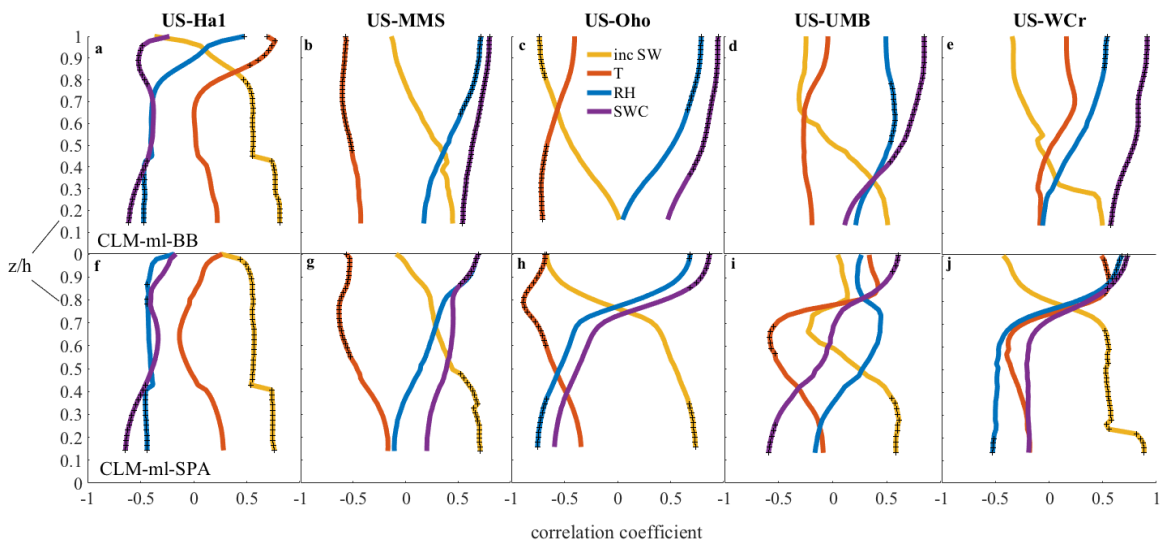
2020JG005658-f01-z-.png



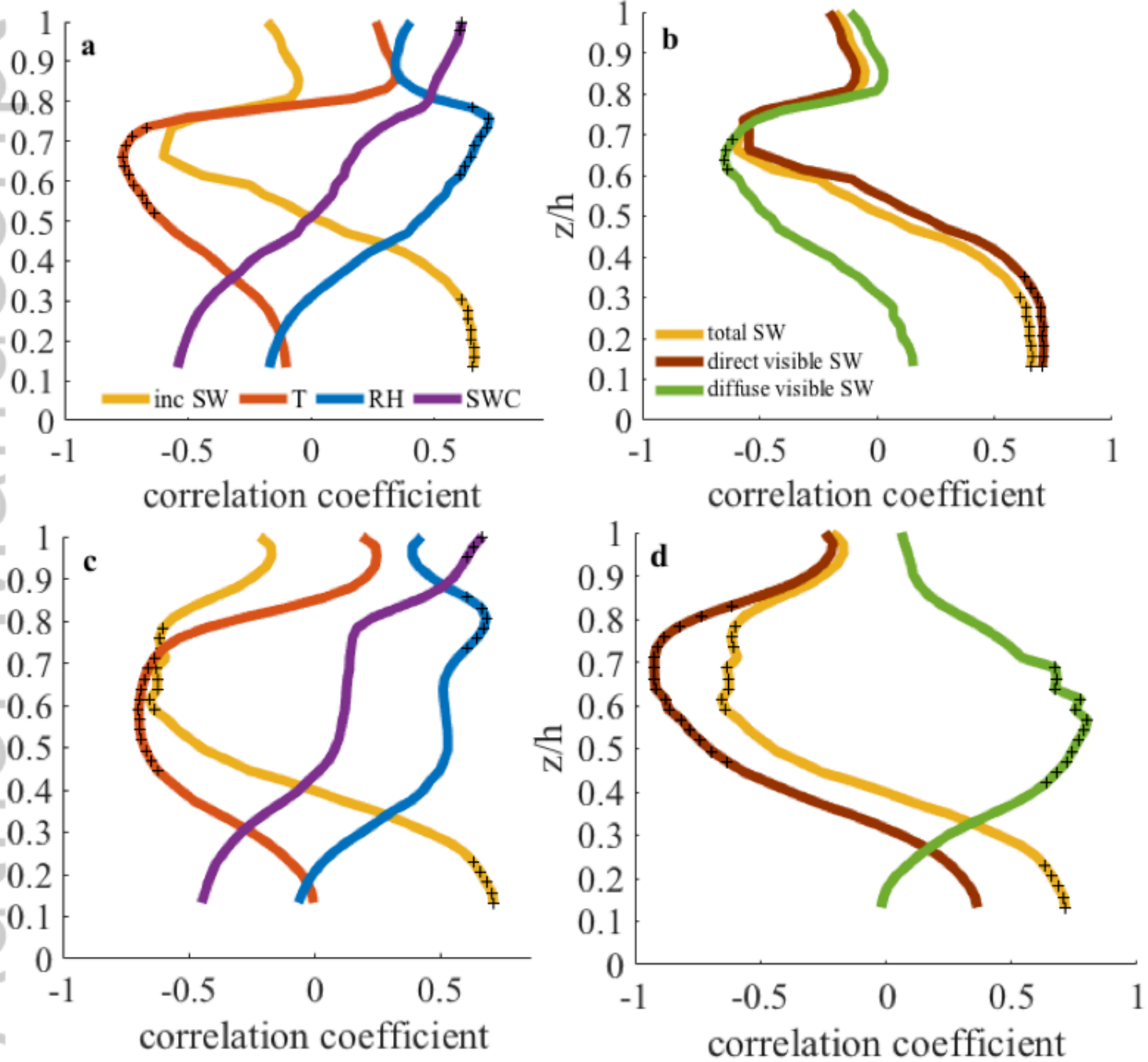
2020JG005658-f02-z-.png



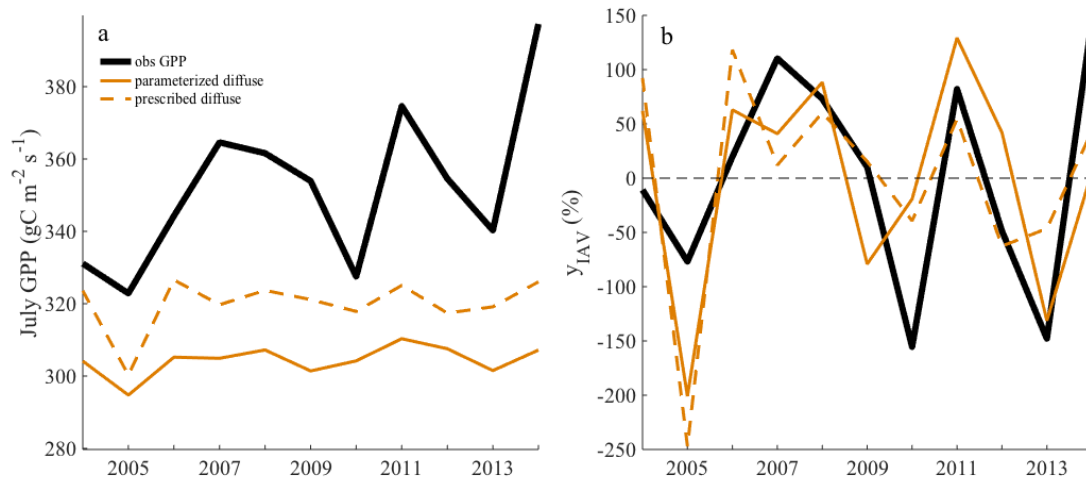
2020JG005658-f03-z.png



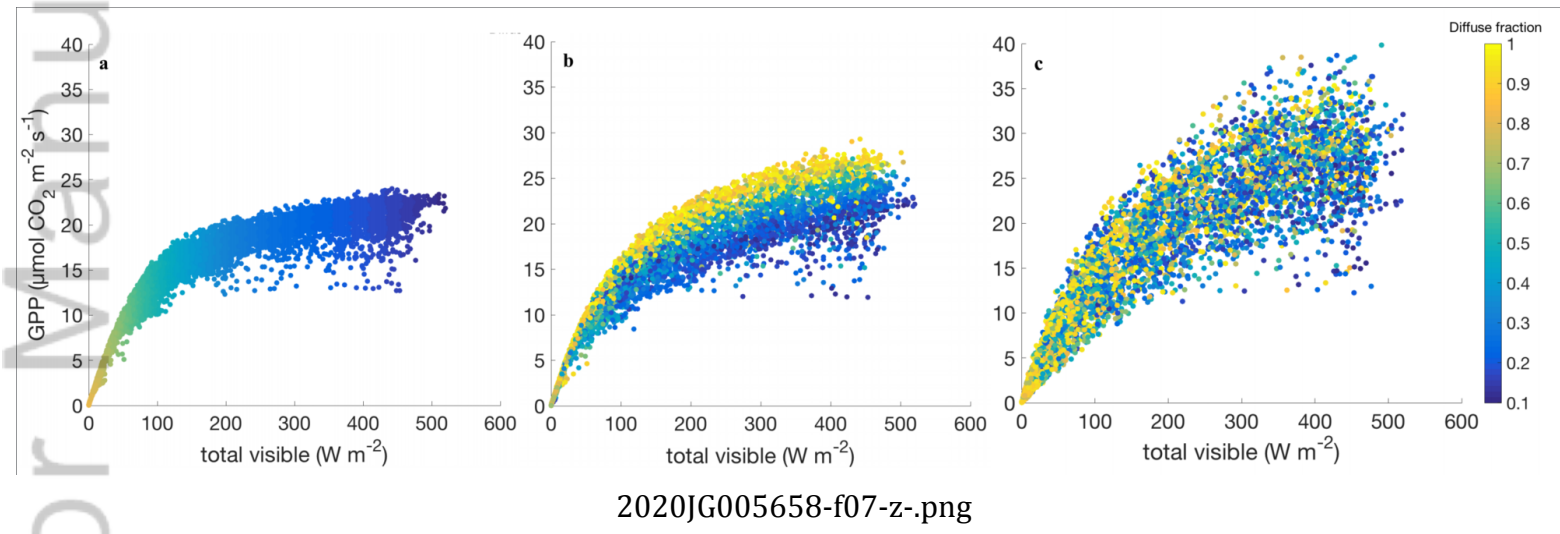
2020JG005658-f04-z-.png



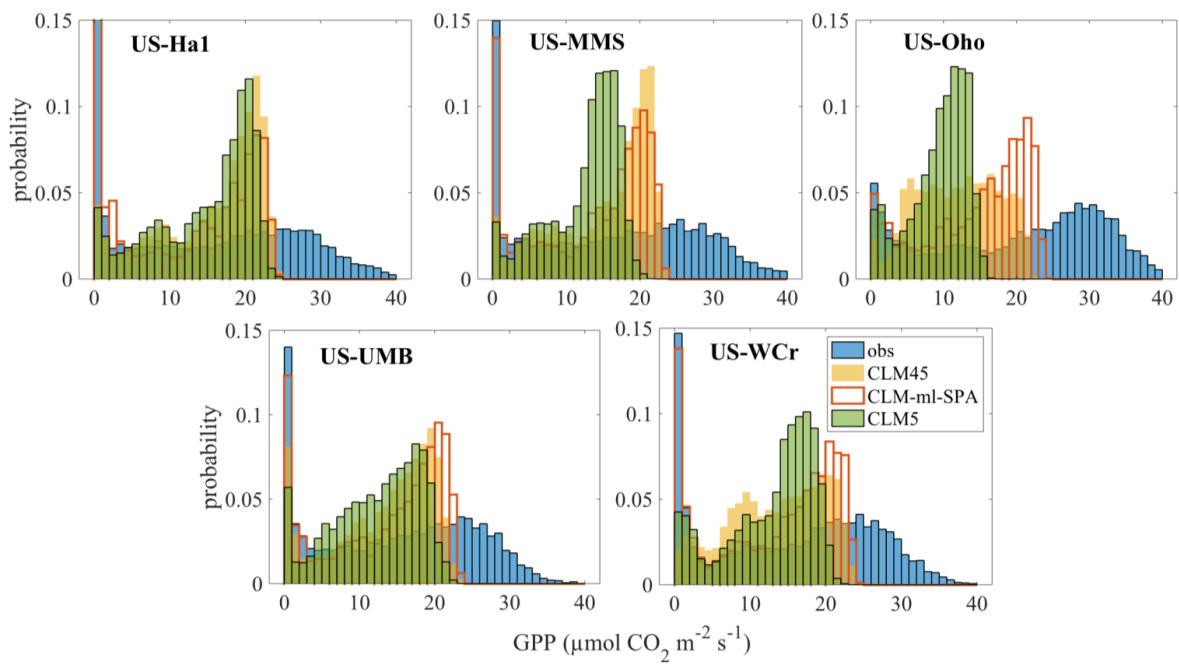
2020JG005658-f05-z-.png



2020JG005658-f06-z-.png



2020JG005658-f07-z-.png



2020JG005658-f08-z-.png